Research Department

Technical Report No. 69

A preliminary study of the impact of C-band scatterometer wind data on global scale numerical weather prediction

Ross N. Hoffman

November 1992

ABSTRACT

A preliminary assessment of the impact of the ERS1 scatterometer wind data on the current ECMWF analysis forecast system has been carried out. The impact of the data is neutral.

This conclusion is based on comparing analyses and forecasts from assimilation cycles which are identical in all respects except that the control experiment blacklists all scatterometer data. Each experiment is comprised of seven days of data assimilation (from 0000 GMT 26 December 1991 through 02 January 1992) and four ten-day forecasts.

At the start of each analysis the current 6 hour forecast (hereafter referred to as the 'first guess') is used as the reference field in the ambiguity removal algorithm (named CREO). Within the statistical interpolation procedures (collectively called OI here), the ERS1 data are thinned to 100 km resolution and a strict quality control on the scatterometer wind directions is imposed. Only 5-10 percent of the thinned CREO winds are rejected for any 6 hour period by OI.

The two sets of analyses are very similar except for the low level wind fields over the ocean. Impacts on the analyzed wind fields are greater over the Southern Ocean, where other data are scarce. For the most part the mass field increments are too small to balance the wind increments. The effect of the nonlinear normal mode initialization on the analysis differences is quite small, but we observe that the differences tend to wash out in the subsequent 6 hour forecast. In the Northern Hemisphere, analysis differences are very small, except directly at the scatterometer locations. In particular the scatterometer data has little impact on the analysis of the storm striking the coast of Norway on New Year's Day.

Forecast comparisons reveal significant differences in the Southern Hemisphere after 72 hours. Notable differences in the Northern Hemisphere do not appear until late in the forecast. Overall the Southern Hemisphere impacts are neutral. Large differences in particular forecast features may be traced backwards in time, but in these experiments, either these features can not be traced back to the initial time or the increments at the initial time are not directly associated with the presence or absence of scatterometer data. We can not reject the hypothesis that the scatterometer data have no direct forecast impact and that the observed forecast impacts are the result of analysis 'noise', i.e., quasi-random differences in the analyses which arise in the assimilation in regions of poor data coverage.

On the other hand the low level wind analysis differences are clearly directly related to the inclusion of the scatterometer data. These differences may in turn be significant when forcing an ocean wave model, or when calculating the atmospheric angular momentum budget. Comparison of the time averaged analyzed wind fields and subsequently of the scatterometer observational increments suggest that, in the Southern Hemisphere, the scatterometer corrects the tendency of the model to overestimate the wind speed under conditions of warm air advection.

The experiments described are preliminary in several respects. In light of expected refinements to the scatterometer model function, the ambiguity removal algorithm and the analysis procedures, we expect these data to ultimately prove useful for numerical weather prediction.

CONTENTS

1. INTRODUCTION

The potential usefulness of satellite borne ocean surface scatterometry to numerical weather prediction has been discussed by *Grantham et al.* (1977), *Cane et al.* (1981) and *Atlas et al.* (1982). This promise may become a reality with the real time data of ERS1, the first European Remote-Sensing Satellite. Previous studies (*Baker et al.*, 1984, *Yu and McPherson*, 1984, *Duffy et al.*, 1984, *Anderson et al.*, 1987, 1991a,b) using large scale numerical weather prediction systems have demonstrated a positive impact in the Southern Hemisphere and negligible impact in the Northern Hemisphere. Further, the Southern Hemisphere impact is greatly reduced if satellite sounding data was already in use, as the addition of the scatterometer data had a much smaller impact. Two studies, using regional scale numerical weather prediction systems, of the exceptional September 1978 storm which damaged the *Queen Elizabeth II* ocean liner, have also been carried out, with generally positive impacts (*Duffy and Atlas*, 1986, *Stoffelen and Cats* 1991). At this writing, one year after launch, we report the first forecast impact studies with ERS1 data to be carried out at ECMWF, the European Centre for Medium Range Weather Forecasts. The impact of the data in the context of currently available satellite data and the current retrieval and analysis procedures is neutral. The work reported here is a necessary (but insufficient) prelude to operational use of the ERS1 scatterometer data.

The experiments described here begin with the operational analysis of 0000 GMT 26 December 1991. The CONTROL and SCATT experiment differ only in that the scatterometer data are blacklisted by CONTROL. For each experiment 28 analyses are performed at 6 hour intervals, beginning with the analysis at 0600 GMT 26 December and continuing until the analysis of 0000 GMT 2 January 1992. For each experiment four ten-day forecasts are made at 36 hour intervals, beginning 60 hours after the start of the experiments, with the forecast of 1200 GMT 28 December. The study period includes the New Year's Day storm which hit the coast of Norway with peak intensity between 0600 and 1200 GMT. The genesis of this storm can be traced back to a depression off Newfoundland at the start of the experiment. In addition, during the last half of the experiment, tropical depression Bryna was developing north of Madagascar. Although there are many data swaths near or hitting these features, actual scatterometer winds for these features are limited, for reasons discussed in Section 2.2.

Before passing to the details of the experiments in Sections 2 and 3, we now highlight the important choices made in the design of our experiments and indicate possible improvements in processing the scatterometer data. We reprocess the basic geophysical measurements - backscatter or σ^0 - into retrieved winds, making use of the first guess as a reference field in CREO. Two important aspects of the retrieval procedures - the model function and the ambiguity removal algorithm - will be further refined in the future. We use the zero degree contour of the operational sea surface temperature (SST) analysis to exclude probable ice points. In the future, it may be possible to use the σ^0 data directly to define a more accurate ice boundary. The retrieved winds at 25 km resolution are thinned to 100 km resolution before being passed to OI. Because

of the possibility that some of the retrieved scatterometer wind vectors are approximately reversed in directions (the so-called '180° ambiguity problem') we impose a severe test to quality control the scatterometer data. We reject any scatterometer wind which differs by 60° or more from the first guess wind. Data which pass this test are assumed to be of very high quality, equal to that of radiosonde winds.

2. METHODOLOGY

For our SCATT experiment, the ERS1 scatterometer data flows from satellite to ground station to ECMWF. At the ground station we may divide the data processing into three steps which respectively produce backscatter measurements (σ^0 values), ambiguous wind vectors, and retrieved wind vectors. The last two steps are performed a second time within our experiments because the ambiguity removal makes use of a reference field. In order to have the most current reference field, which itself incorporates previous scatterometer data, we use the first guess fields of the experiment. Since the real time ERS1 data do not include ambiguities, these must be recreated as well. Once the wind retrievals are available they are passed to OI which performs quality control and statistical interpolation of the data. The resulting analysis then provides the initial condition for the 6 hour forecast which becomes the reference field for the next batch of data.

2.1 ERS1 σ^0 Data

The ERS1 scatterometer observes the C-band radar backscatter at the earth's surface (*Francis et al.*, 1991). The ERS1 satellite is in a sun synchronous polar orbit with inclination 98.5° and a descending equatorial node at 1030 local time. Its orbital period is approximately 100 minutes, its nominal ground speed is 6.67 km/s and its nominal altitude is 780 km. With slight shifts in altitude, the ERS1 satellite may execute 3, 35 or 176 day repeat patterns. The scatterometer instrument uses three antennas pointing at angles of 45°, 90° and 135° from the satellite direction of travel, in the horizontal plane, to observe a swath of data 500 km wide beginning 200 km from the satellite subtrack. The data swath corresponds to incidence angles at the earth's surface of 18° to 47° for the mid beam and 25° to 59° for the fore and aft beams. The scatterometer transmits a linearly vertically polarized signal at 5.3 GHz. The nominal field of view illuminated at the surface is 50 km by 50 km. Data is obtained with a grid spacing of 25 km in 19 cells perpendicular to the satellite path. The center of cell 1 is 225 km from nadir and the center of cell 19 is 675 km from nadir. At each location there are nominally 3 σ^0 measurements, one from each antenna, observed within time span of approximately 70 to 200 seconds, increasing with incidence angle. The scatterometer is turned off when the synthetic aperture radar operates. Turning the scatterometer on or off produces regions of 1 or 2 beam operation.

The data are packaged into products of 19 cells by 19 rows. In the work described here these data products are thinned to either 50 km or 100 km resolution. The 50 km resolution data is obtained by retaining data within each product for cells and rows 1, 3, 5, ... 19 only. For 100 km data, only cells and rows 3, 7, 11, 15, and 19 are kept. The data volumes for 25:50:100 km resolution are therefore 361:100:25 per data product. The data coverage patterns produced by this thinning procedure is shown in Fig. 1.

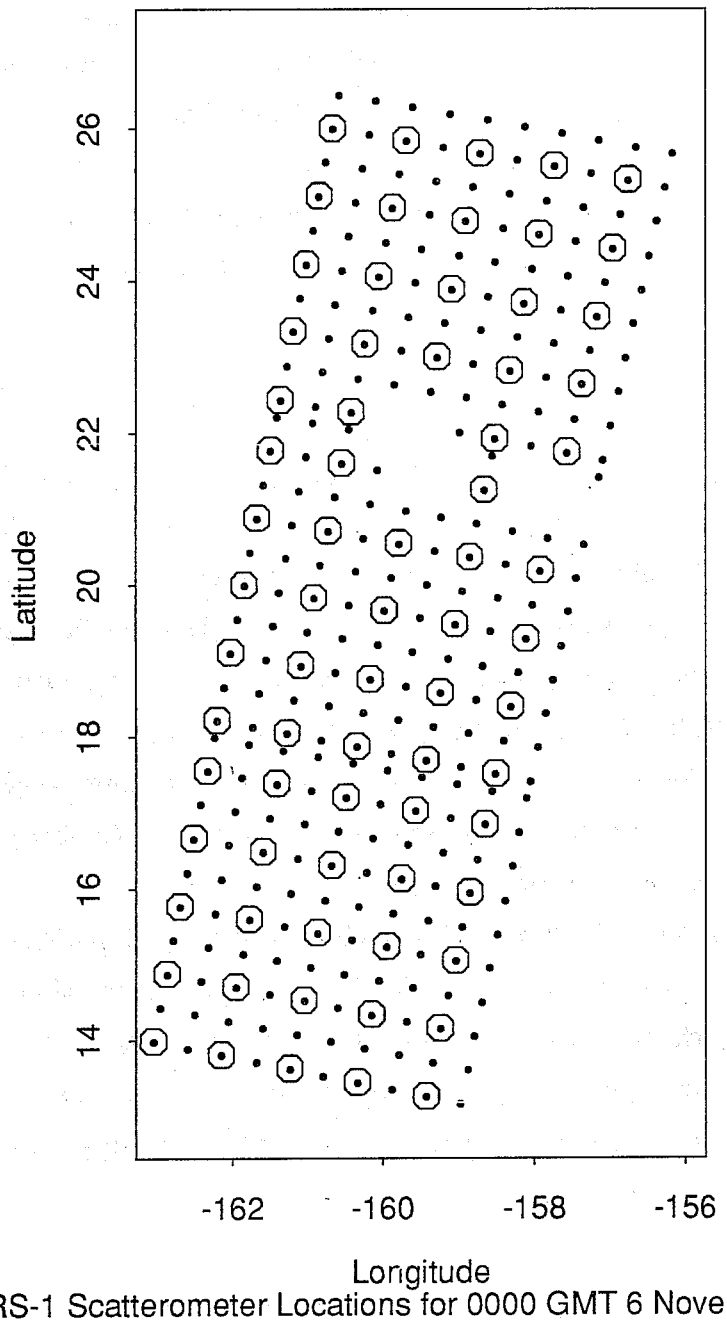

Fig. 1 Data coverage for 50 km resolution data (dots) and 100 km resolution data (circles). Missing data in the middle of the swath is due to the presence of land (Hawaii). These are the data for the first three data products in the 6 hour window centered on 0000 GMT 6 November 1991.

The satellite was launched 0146 GMT 17 July 1991. Real time σ^0 data before 4 November 1991 are affected by calibration errors. Since that time an improved calibration based on tropical rain forest data has been in use. The amount of data per day archived at ECMWF for the three months beginning with November 1991, is shown in Fig. 2. As can be seen, data coverage during the study period is as good or better than other weeks. The absence of data during the middle of December corresponds to an orbit shift. In mid January, ground station Kiruna (Sweden) failed to process scatterometer data. Excluding orbit shifts, the coverage shown is fairly typical of subsequent months as well. Thus, at 100 km resolution for a 6 hour period, we normally expect approximately 4000 ocean observations. However, for reasons described below, CREO produces winds at only about half of these locations and a further 5-10% of the data are rejected by OI. Thus only about 2000 scatterometer wind observations per 6 hour period are ultimately used by OI in creating the analyses described here.

Data coverage for one 6 hour period at the start of one of our forecast cases is shown in Fig. 3. Regions of 1 and 2 beam operation are orange and red. Data locations with no σ^0 data are yellow. When 3 σ^0 values are present, the colors describe the results of the CREO as applied in real time (i.e., results determined at the ground stations). Locations with no retrieved winds are black. These are likely low wind speed cases. Green, blue and purple correspond to the three possible modes of wind retrieval - autonomous, meteorological background, rank 1 - described in Section 2.2.

2.2 Scatterometer wind retrieval

At each data location having 2 or 3 σ^0 observation, 2 to 6 but usually 4 ambiguous wind vectors may be retrieved (*Price*, 1976). In this study winds are retrieved only for locations with 3 σ^0 observations. The ambiguities are the minima of a cost function, which is a function of wind speed and direction, measuring the difference between the observed σ^0 and those calculated for the given wind speed and direction. Three example are given in Fig. 4. Relative minima not sufficiently small are ignored. Thus if the σ^0 data are very inconsistent there may be no ambiguities. Also, no ambiguities are produced at low wind speed since the returned radar signal is too weak to determine wind direction accurately. In our experiments the minimum retrieved wind speed is 2 m/s. (The corresponding cutoff for real time data is 4 m/s.)

The calculation of the σ^0 values given wind speed and direction (and given constants describing the geometry of the observation) has been termed the model function. (Such functions are often termed the forward problem to distinguish them from the retrieval or inverse problem.) Two prelaunch versions of the ERS1 C-band model function called CMOD1 and CMOD2 were developed by *Long* (1985, 1991). Since launch several new model functions have been proposed. The one used here is called CMOD2_Z and was generated by matching observed σ^0 values with the ECMWF operational analyses of 10 m winds (*Stoffelen and Anderson*, 1992). Fig. 5 describes these model functions. We have found in preliminary experiments

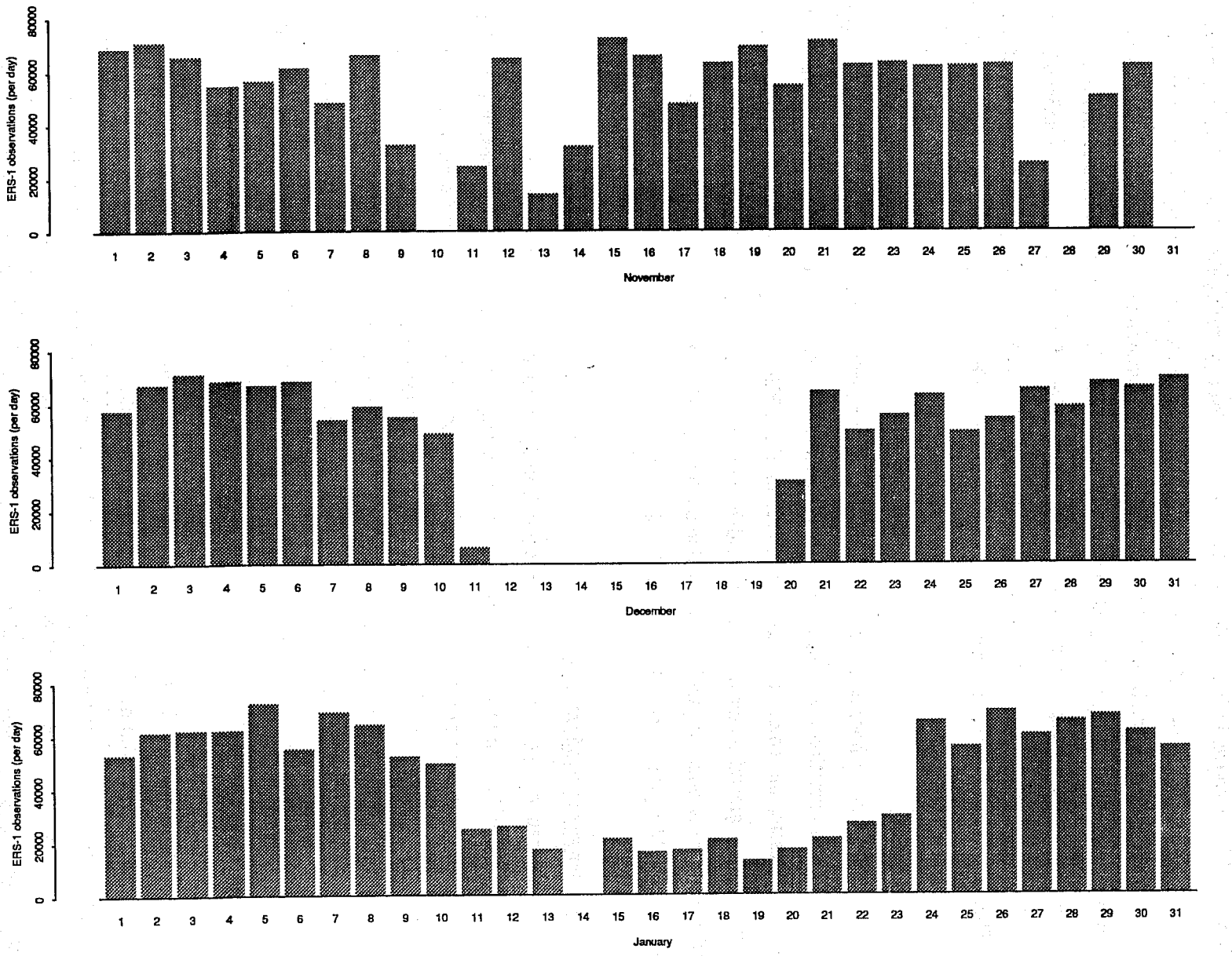

Fig. 2 Number of ERS1 observations per day for November 1991 through January 1992. These counts correspond to 50 km resolution data and exclude observations over land.

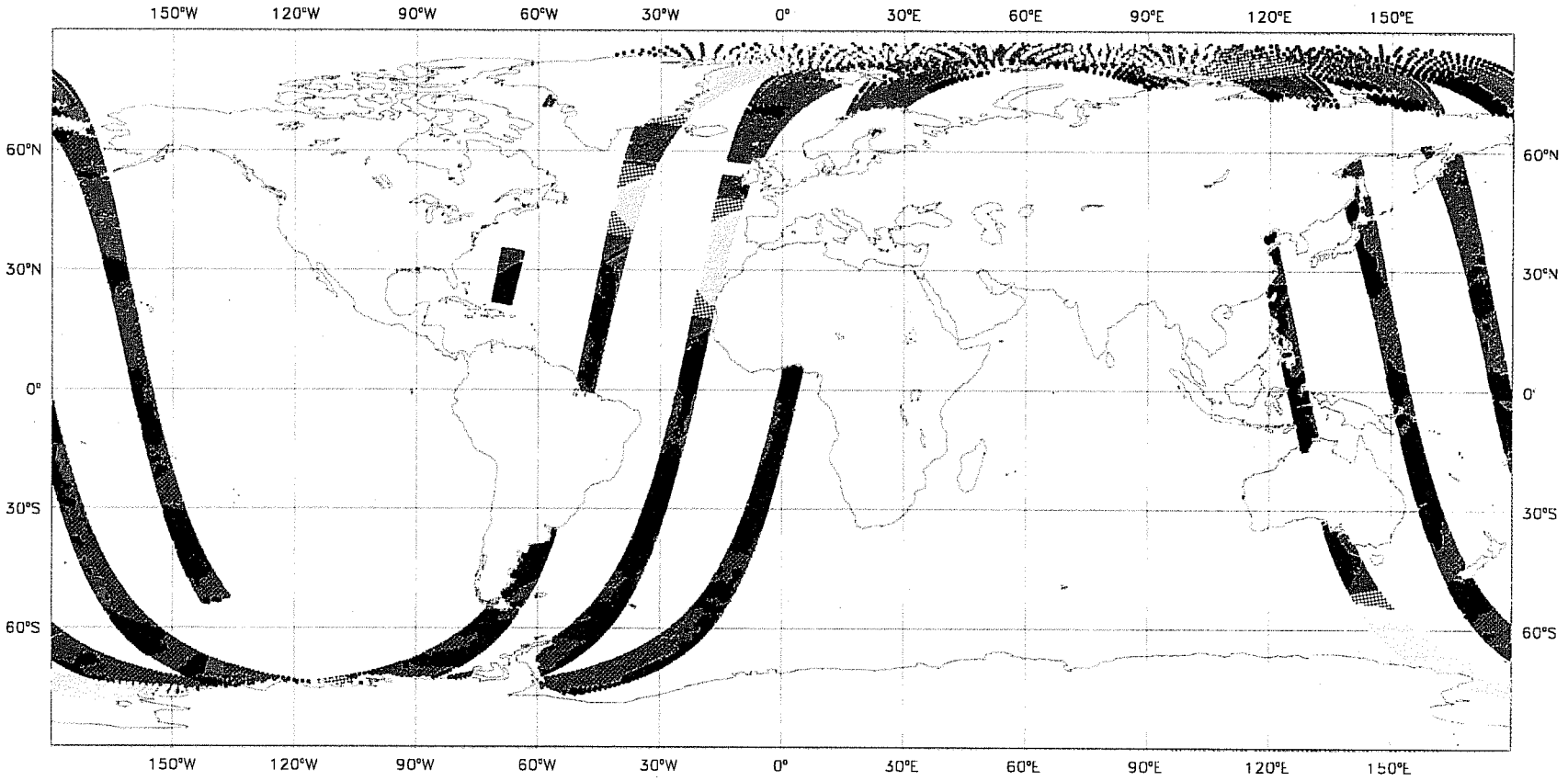

Fig. 3 ERS1 data coverage for 1200 GMT 31 December 1991. The data have been thinned to 50 km resolution and observations over land are excluded. The color coding is explained in the text.

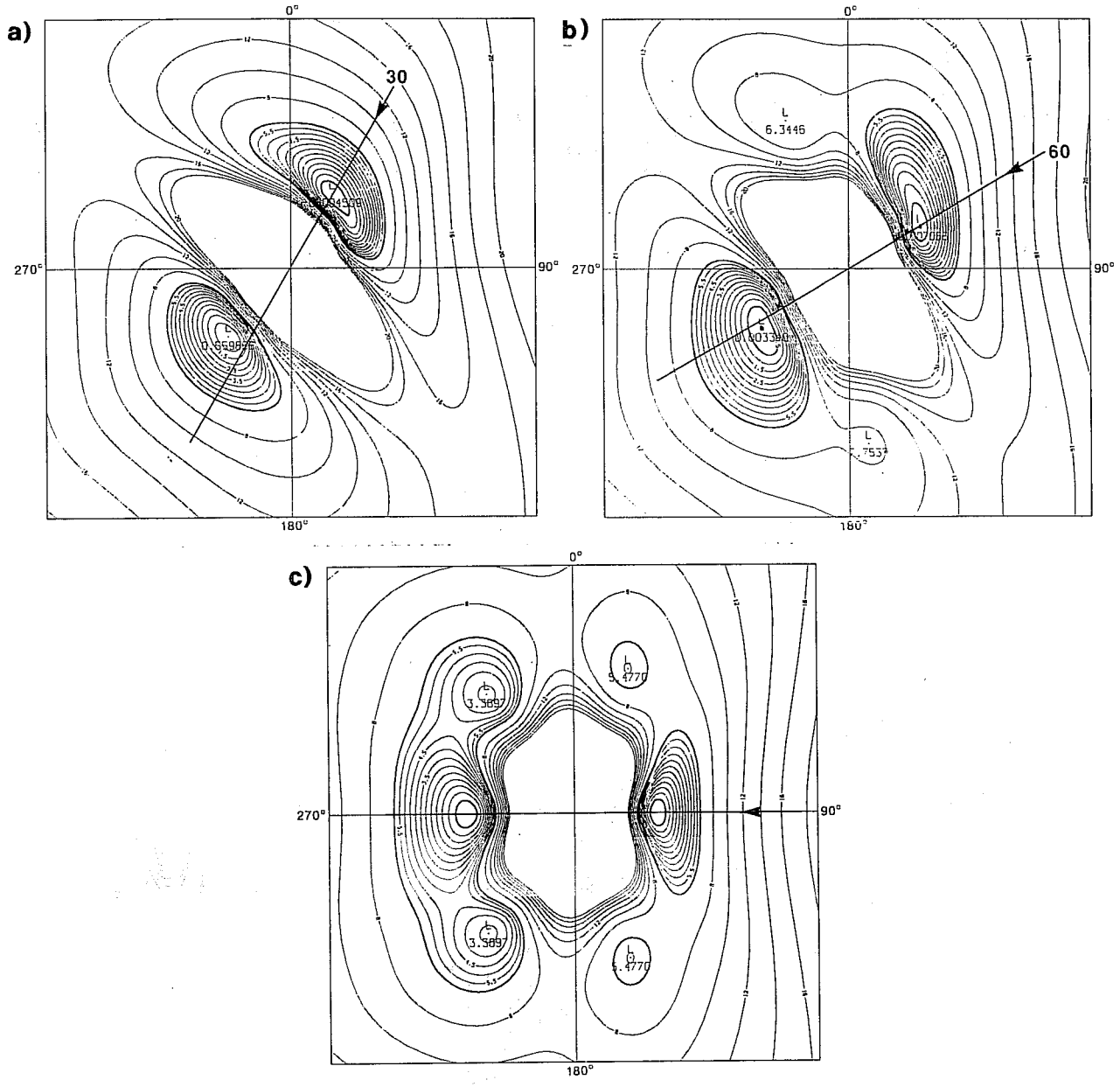

Fig. 4 The cost function, as a function of wind components in the coordinate system defined by the satellite forward motion, for triplets of noiseless σ^0 measurements evaluated using CMOD1. The true wind speed is 10 m/s and the wind direction is from (a) 30° (b) 60° and (c) 90° measured clockwise from the satellite direction. Note that the contour interval is smaller near the minima and that no contours are drawn close to the origin where the cost function is very high. After *Graham et al.* (1989).

that, due to the sensitivity of the ambiguity removal scheme, different model functions, can result in very marked changes in the retrieved winds.

Each ambiguity is assigned a probability of being the closest (i.e., the closest ambiguity to the true wind vector). Ambiguities with small relative minima are more likely. The highest probability ambiguity is termed the rank 1 solution. The first method of ambiguity removal is to choose the rank 1 solution at all points. Usually only the probabilities of the rank 1 and rank 2 solutions are large, and the associated ambiguous wind vectors point in nearly opposite directions. Various filtering approaches may then be used to extract a horizontally consistent pattern. In autonomous mode (i.e. with no other data), these schemes achieve 98 or 99 percent accuracy in simulation under the conditions that the rank 1 solution is in fact the closest to the correct solution for 60% or more of the time and that there is no horizontal coherence to the pattern of locations where the rank 1 solution is not the closest (*Schultz*, 1990). Unfortunately results at the ECMWF (*Stoffelen et al.*, 1992) show that the ERS1 instrument skill (percent of most likely which are closest) is less than 50%. In this situation meteorological background information must be used for reference. The autonomous ambiguity removal algorithm in CREO produces two horizontally consistent fields by filtering the ambiguous winds. In our experiments, CREO then chooses the field which agrees best with the reference wind field. If neither CREO field agrees with the reference field, no retrievals are produced. In nominal operation of CREO, a series of tests determines which mode of ambiguity removal is used at each point. In our experiments CREO is forced to always operate in the meteorological background mode. A complete description of CREO is given by *Cavanié and Lecomte* (1987a,b) and by *Graham et al.* (1989).

Anomalous wind retrievals are obtained over ice. To filter ice points CREO excludes all points for which the operational SST analysis, either at 6 h or 48 h previous to the current analysis time, is less than 0°C. Once identified, these points are treated as if they were land. Since sea water, depending on its salinity, remains unfrozen at temperatures above about -1.7°C this is a conservative criterion. However partial ice cover and potential errors in the SST analysis must be allowed for. A small number of ice points may pass through this filter, but such points will often fail the OI quality control described below because the 'wind' retrievals over ice are in many cases quite different from adjoining wind retrievals over open ocean.

2.3 Scatterometer Wind Direction Quality Control

Quality control of scatterometer winds is vital. Retrieved scatterometer winds can have gross errors due to problems with ambiguity removal or the presence of ice. In addition, at low incidence angles, at the inner edge of the swath, directional errors are larger. (See Fig. 8 below.) Scatterometer data quality control takes place both in CREO and in OI. In both cases a comparison of the retrieved wind directions to the first guess provides the critical quality control.

The CMOD2 Model Formulation and Coefficients

The form of the CMOD2 model is:

$$\sigma^{o}_{lin} = b_0.(1 + b_1 \cos\phi + b_2 \cos 2\phi)$$

where:

$$b_0 = 10^{\alpha}.V^{\gamma}$$

α, γ, b_1 and b_2 are expanded as Legendre polynomials to a total of 24 coefficients (some of which may be zero):

$$\begin{aligned}
\alpha &= c_1P_0 + c_2P_1 + c_3P_2 + c_4P_3 \\
\gamma &= c_5P_0 + c_6P_1 + c_7P_2 + c_8P_3 \\
b_1 &= c_9P_0 + c_{10}P_1 + c_{11}P_2 + c_{12}P_3 + (c_{13}P_0 + c_{14}P_1 + c_{15}P_2 + c_{16}P_3).V \\
b_2 &= c_{17}P_0 + c_{18}P_1 + c_{19}P_2 + c_{20}P_3 + (c_{21}P_0 + c_{22}P_1 + c_{23}P_2 + c_{24}P_3).V
\end{aligned}$$

where the Legendre polynomals in are:

$$P_0 = 1 \quad P_1 = x \quad P_2 = (3x^2 - 1)/2 \quad P_3 = (5x^2 - 3).x/2 \quad \text{with } x = (\theta - 40)/25$$

V is the wind speed in ms^{-1}, ϕ the relative wind direction in degrees and θ the incidence angle in degrees.

CMOD2 Legendre polynomial coefficients

Model:		CMOD2	CMOD2_Z	CMOD2_I2	CMOD2_M3
α	c_1	-2.217986	-2.323300	-2.303908	-2.376829
	c_2	-1.769950	-1.637100	-1.616729	-1.719836
	c_3	0.296464	0.625300	0.569954	0.575082
	c_4	0.000000	0.000000	0.000000	-0.019508
γ	c_5	1.068610	1.188500	1.196991	1.163113
	c_6	0.652920	0.620800	0.641966	0.582905
	c_7	0.044130	-0.116700	-0.073403	-0.161615
	c_8	0.000000	0.000000	0.000000	-0.083153
b_1	c_9	0.137300	0.137300	0.046764	0.026213
	c_{10}	0.162000	0.162000	0.143697	0.165012
	c_{11}	0.000000	0.000000	0.015089	-0.052105
	c_{12}	0.000000	0.000000	0.000000	0.075827
	c_{13}	-0.000709	-0.000709	0.003395	0.000000
	c_{14}	0.000000	0.000000	-0.005760	0.000000
	c_{15}	0.000000	0.000000	-0.003531	0.000000
	c_{16}	0.000000	0.000000	0.000000	0.000000
b_2	c_{17}	0.404800	0.404800	0.247040	0.334217
	c_{18}	0.161600	0.161600	0.128905	0.163288
	c_{19}	-0.065200	-0.065200	-0.031911	-0.043359
	c_{20}	0.000000	0.000000	0.000000	-0.051932
	c_{21}	0.000000	0.000000	0.004800	0.000000
	c_{22}	0.000000	0.000000	0.002695	0.000000
	c_{23}	0.000000	0.000000	-0.003959	0.000000
	c_{24}	0.000000	0.000000	0.000000	0.000000

Fig. 5 Specification of CMOD2, CMOD2_Z and three other candidate model functions (*Offiler*, pers. comm., 10 April 1992).

As we have seen in the previous section there are a number of conditions under which CREO will not retrieve winds. In practice about half of the ocean points observed by ERS1 will not have a wind observation. Many of these are over ice (i.e., SST < 0) or at locations where the wind speed is low (< 2 m/s). There are a few cases when the σ^0 observations are inconsistent. Finally, a number of winds are rejected by CREO because both fields produced by filtering the ambiguities are far from the reference field.

Within OI, all data including the scatterometer winds, pass through three phases of quality control. In each phase a number of test statistics are calculated and examined. For each test statistic there are normally three critical values, dividing the data into four categories - correct, probably correct, probably incorrect and incorrect. The first phase, the preliminary check, makes sure the observed values are physically reasonable. For example, surface winds in excess of 150 m/s are sure to be rejected. The second phase, compares the observed values to the first guess. In the OI, for winds the first guess test statistics are the magnitude of the vector wind difference normalized by the expected standard deviation of such a difference and the wind direction difference. The critical values for these tests are (2.83, 4.24, 4.47) and (60, 90, 120). At ECMWF, the wind direction check is normally applied only to data above 700 mb and for winds in excess of 15 m/s. Here we apply the wind direction check to all scatterometer winds. The third phase, the OI check, compares the observation to an analysis at the observation point made without the observation in question (*Lorenc*, 1981).

OI treats scatterometer observations as a type of buoy. Incorrect buoy observations are rejected, but those classed as probably incorrect by only one of these tests are retained. Thus, the extreme critical value of these tests statistics is of most importance here. (In some cases the results of different tests are combined. For example, in our experiments, the occasional scatterometer observation is rejected because both the wind vector and wind direction check classify the data as probably incorrect.) Using the criteria developed for buoys very few scatterometer data are rejected. We expect that ERS1 data will almost always pass the preliminary and OI checks. With regard to the preliminary check, since there is no human intervention, there is little chance of gross errors. Further, the OI check is not expected to be very effective for the scatterometer, since incorrect scatterometer observations will occur mainly as patches of direction reversals. Consequently, the OI quality control of scatterometer data relies on the first guess. Preliminary experiments showed that few scatterometer winds are rejected by the wind vector comparison even after decreasing the critical values to one third of the nominal values listed above and after decreasing the estimated observational errors to match that of radiosondes. For scatterometer data we tightened the critical values in the directional check to (30,45,60), so that a difference of 60° or more is classed incorrect. This choice was made on an ad hoc basis - that we wished to be conservative and that few wind direction differences are near 90°, so any critical value in the range of 60° to 120° is reasonable.

Results from our experiment show that the OI directional quality control as implemented is acceptable. First, only 5-10 per cent of the winds produced by CREO are rejected by OI (see Fig. 6). Almost all of these rejections are due to the directional check, and the majority of these are for low wind speeds (< 6 m/s) (see Fig. 7). A number of the rejected data are in the subtropics for cases where the scatterometer winds have a confused directional pattern. Problems with scatterometer wind directions are expected to be worse at low wind speed, as we can see in this figure and for low incidence angle as can be seen in Fig. 8. After the analysis, neighbouring scatterometer data tend to validate some of the marginally rejected data. This is seen in Fig. 9 which shows scatterplots of wind direction increments before and after the analysis of 1200 GMT 31 December 1991. In both panels of this figure only data failing the direction check in SCATT are plotted. Note that in the CONTROL, few of these data are better fit after the analysis, indicating there is no neighbouring data of other types corroborating the scatterometer data.

2.4 ECMWF Data Assimilation System

The aim of this section is to provide a thumb nail description of the ECMWF data assimilation and forecast system, and to describe some aspects of the system which are particularly relevant to our experiments. The ECMWF system is constantly evolving and there are several versions in use at any one time. The version of the forecast model used is known as cycle 41 and the library versions of the analysis software are those of 31 March 1992. T106 spectral resolution, 19 levels in the vertical and a full Gaussian grid are used.

The ECMWF data assimilation system is based on the 3D statistical interpolation of observation minus first guess differences. These differences are called the observation increments. The statistical interpolation is basically a regression analysis, with no constant term, in which the covariances needed to define the normal equations are calculated from simple empirical parametrizations. The OI is multivariate in wind and mass (geopotential height, thickness) and univariate in relative humidity. The analysis uses observations from radiosondes, pilot and constant level balloons, aircraft and dropsondes, ships, moored and drifting buoys, surface stations, and satellites. The satellite observations used in our experiments, besides the scatterometer winds, include cloud drift winds from geostationary platforms and layer thicknesses from TOVS, the TIROS Operational Vertical Sounder. Below 100 mb, the TOVS data are used only in the Southern Hemisphere. The distinguishing feature of the ECMWF OI is the use of analysis volumes. This makes the analysis less sensitive to data selection. The assimilation system has evolved since *Lorenc's* (1981) basic description with reformulations and extensions described by *Shaw et al.* (1987), *Lönnberg et al.* (1988), *Lönnberg* (1988) and *Undén* (1989). A complete and up to date description of the assimilation system is provided by ECMWF Research Manual No. 1 (*Lönnberg et al.*, 1992). The analysis is initialized by a diabatic nonlinear normal mode initialization (*Wergen*, 1987). This procedure initializes only the first five vertical modes, using two iterations of a *Machenhauer* (1977) scheme. The filtered estimate of the diabatic forcing is held constant during the iteration. A six hour forecast from the initialized analysis provides the first guess for

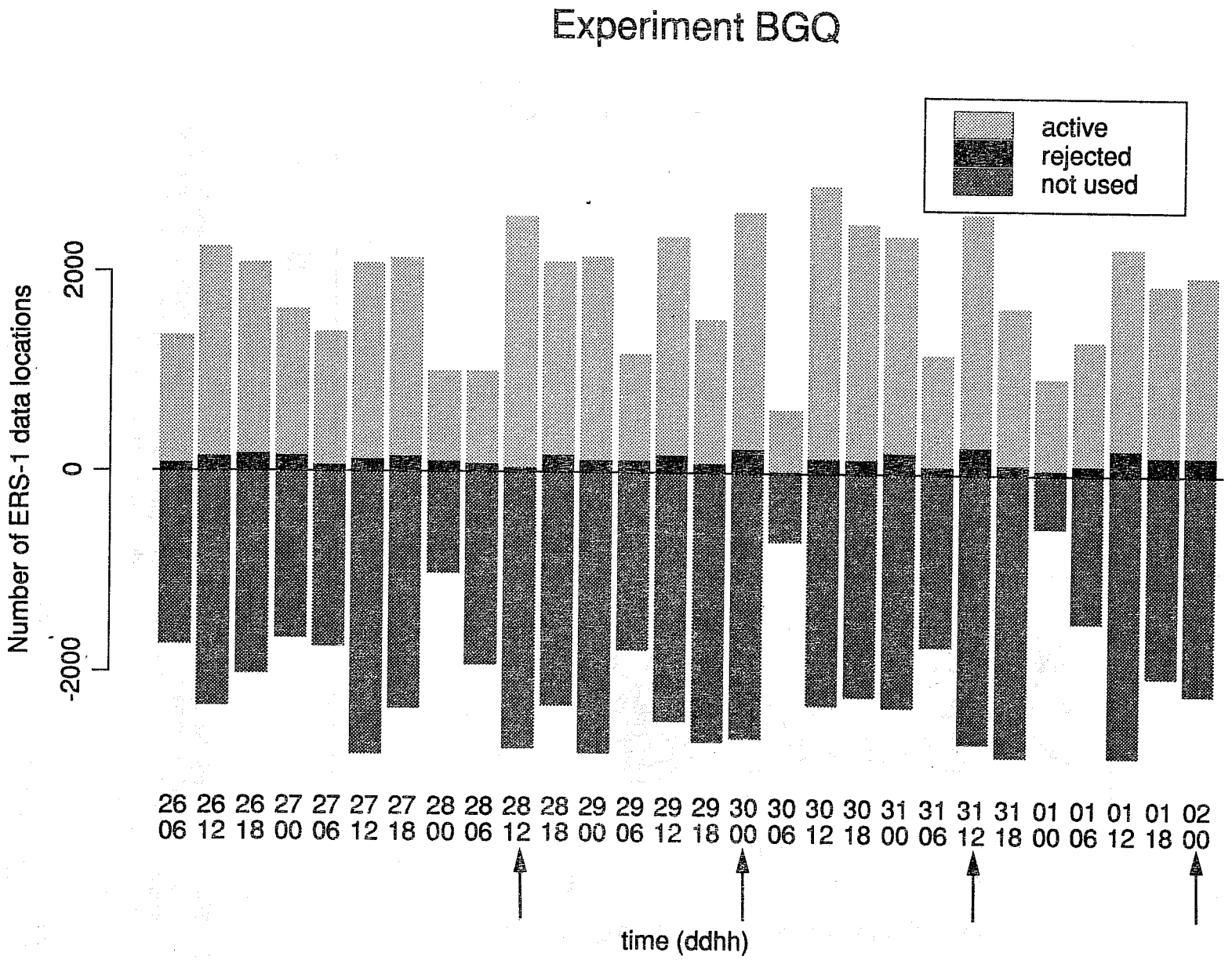

Fig. 6 For each analysis time, the number of ERS1 data used and not used by the OI in the SCATT analyses are plotted above and below the zero line. Of those used, the number rejected by the OI quality control is shown. Arrows point to the times at the start of the four forecasts.

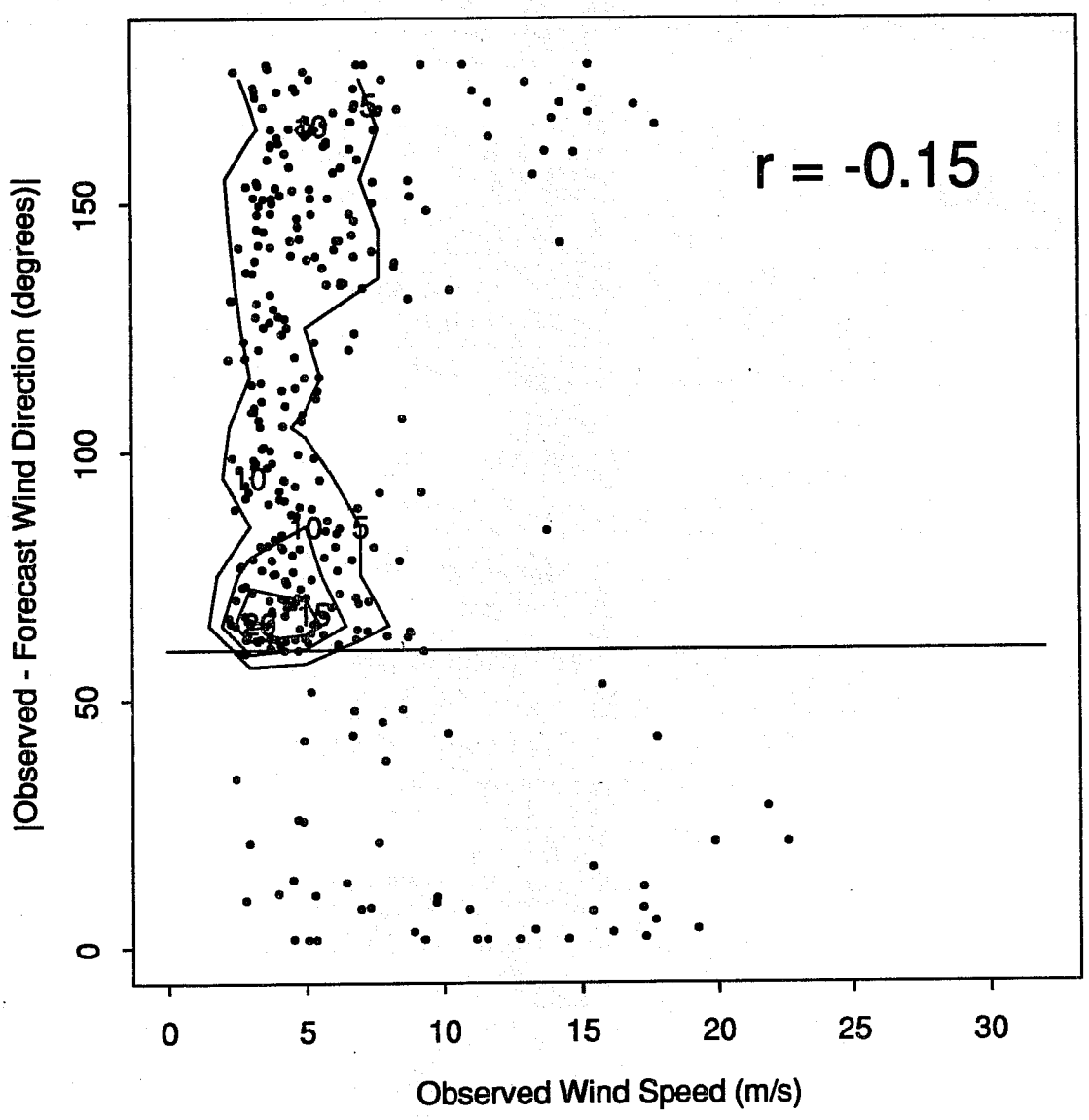

Fig. 7 The ERS1 data rejected by the OI quality control at 1200 GMT 31 December plotted in terms of the absolute wind direction difference between the scatterometer and the first guess and the scatterometer wind speed. The horizontal line indicates the critical value of 60°. (In this and subsequent scatter plots, r indicates the correlation coefficient and contours are drawn for a 2 dimensional histogram of the data.

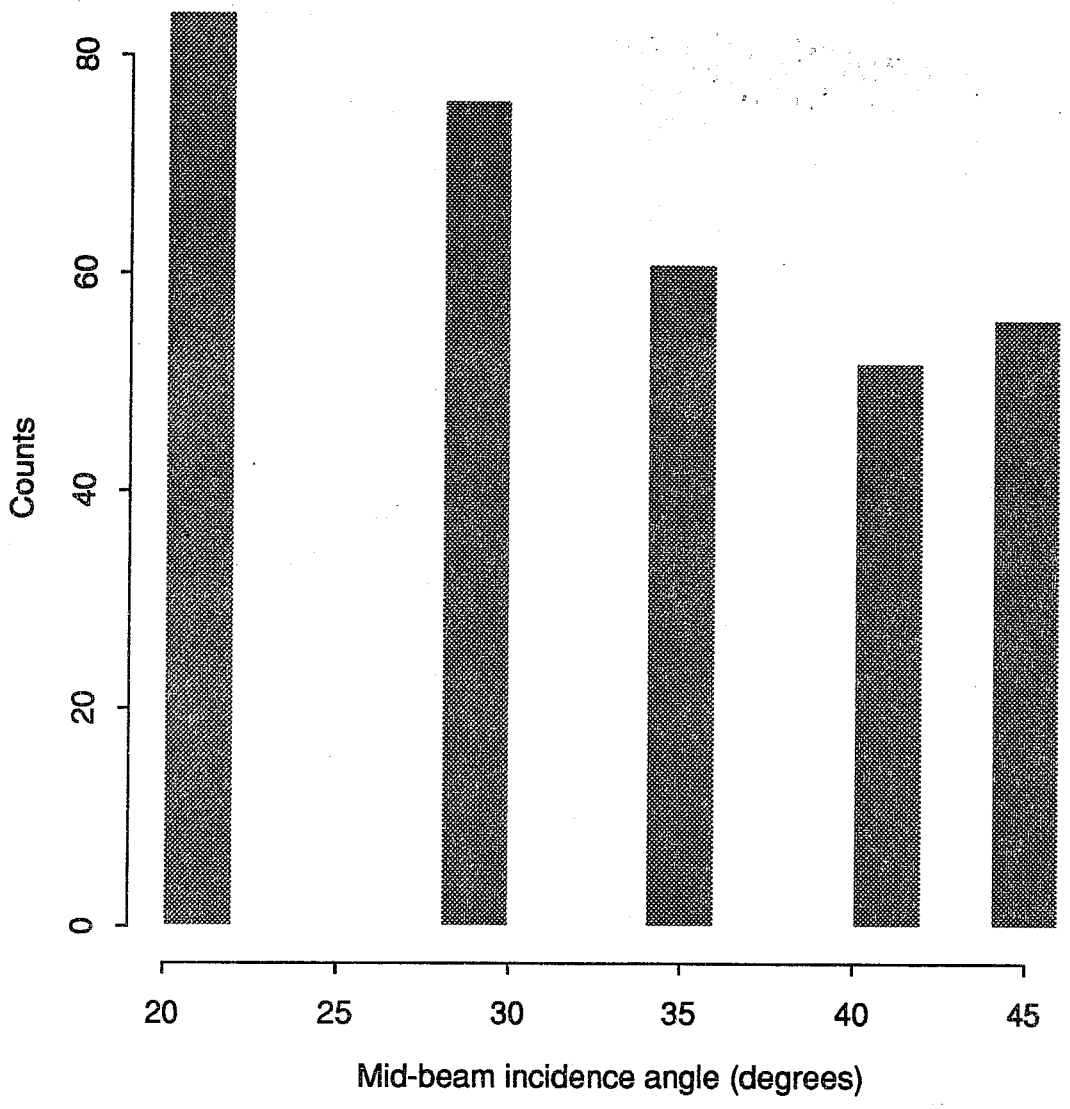

Fig. 8 The number of ERS1 data failing the OI quality control as a function of incidence angle. Note there are only 5 cells retained for the 100 km resolution data. This is the same data sample as in Fig. 7.

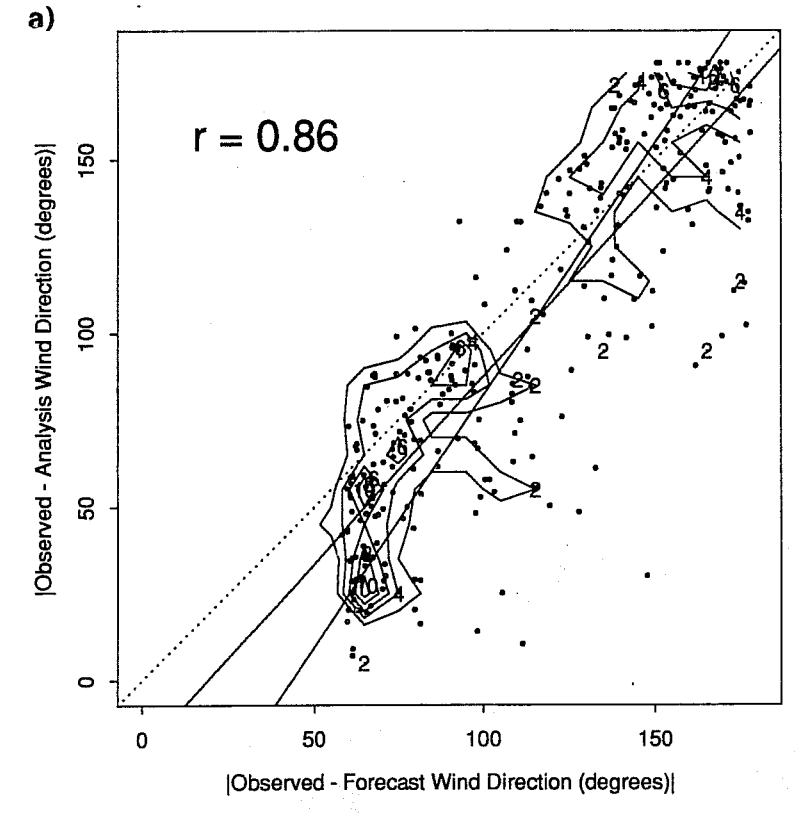

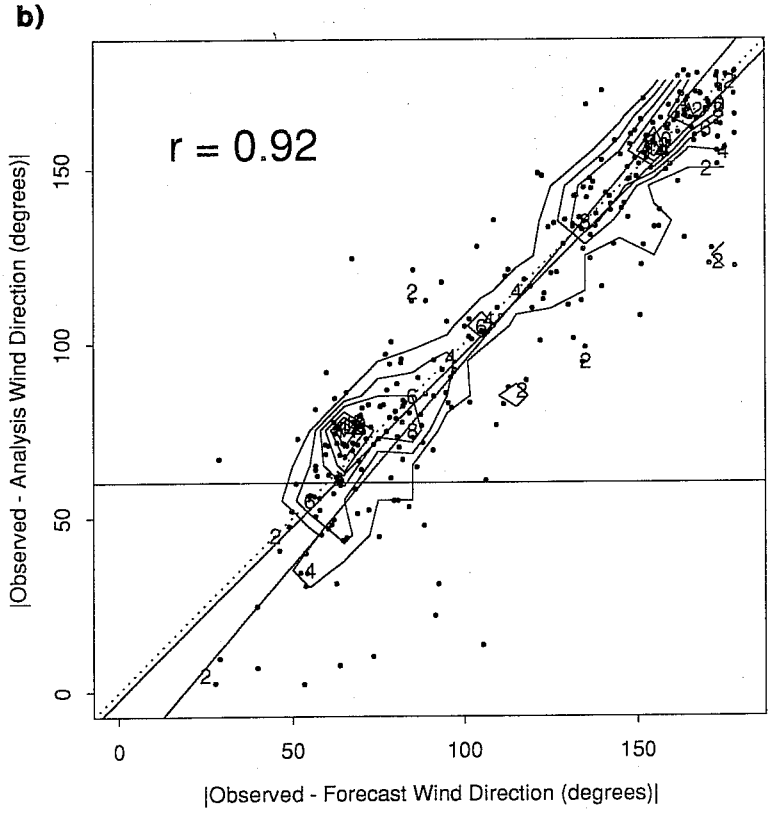

Fig. 9 Scatterplots of absolute wind direction differences before and after the OI for (a) the SCATT experiment and (b) the CONTROL experiment. Only ERS1 data failing the directional check in the SCATT experiment are plotted. These are the data points in the upper part of Fig. 7. (Three lines are drawn for reference here, as well as in some of the following scatter plots. These are the lines representing x=y, y regressed on x and x regressed on y.)

the next analysis. The six hour forecast is actually extended to nine hours and the first guess fields at 3, 6 and 9 hours are interpolated linearly in latitude, longitude and time to the observation locations and times.

The ECMWF forecast model used to generate the first guess and 10-day forecasts in our experiments is a primitive equation hybrid coordinate global spectral model with comprehensive physics (*Simmons et al.*, 1989). The boundary layer parametrization is the bulk parametrization described by *Louis* (1979). Treatment of the ocean is rather simple. Over the ocean, the lower boundary conditions are zero velocity, a prescribed SST and the saturation mixing ratio associated with the prescribed SST. There are no waves. In our experiments, the model resolution is T106, with a corresponding Gaussian grid, used for the physics calculations, of 1.125° longitude by approximately 1.121° latitude. This grid is approximately 125 km square at the equator. In the vertical 19 layers are used. The resolution in the lower part of the atmosphere (up to 700 mb) is roughly 50 mb. In addition, there is one layer very close to the surface at approximately 32 meters above the surface. We note that the analysis is performed on the three dimensional grid of the model, i.e. 125 km resolution in the horizontal and 19 levels in the vertical.

The effective resolutions of the model and analysis are much coarser than the 125 km computational grid. First, the smallest scale (i.e. the smallest half wavelength) representable by the spectral coefficients is approximately 200 km. Secondly, in the case of the model, diffusion further limits the scales present. Similarly, the analysis changes are restricted to larger scales by the horizontal structure functions used. For archiving a T106 experiment, a T63 representation would be adequate for most uses. We will henceforth refer to the model and analysis as having 200 km resolution, but this discussion must be kept in mind.

There are certain aspects of OI which directly relate to the use of scatterometer data, or indeed any particular sort of data. These are the quality control, data selection, and observational error statistics. Also, since the analysis is the result of balancing the fit to the observations and the first guess, the forecast error statistics must be considered. We have already discussed the quality control in Section 2.3. The three other topics will be discussed briefly here.

2.4.1 *Observational error statistics*

In our experiments, errors in the scatterometer u and v wind components are assumed to be normal, unbiased and uncorrelated with a standard deviation (in each component) of 2.0 m/s. None of these assumptions hold exactly.

For scatterometer winds, there is a strong interaction between quality control and the observational error statistics. Before quality control the distribution of errors is very non Gaussian, because of the ambiguity problem, and with strong horizontal correlations, because errors in ambiguity removal will affect patches of data. After the quality control these problems are much less. There is still a problem with directional

errors at the inner edge of the swath being correlated in the along track direction. Further, inadequacies in the model function related to geophysical phenomena, such as wave characteristics, might induce horizontal correlations. Nevertheless, in our experiments the ERS1 data errors are modeled as normal, unbiased and uncorrelated.

The standard deviation used in OI (called estimated observational errors or simply errors here) for near surface wind components varies from 2.0 m/s for radiosonde winds to 3.0 m/s for airline and cloud track winds to 3.6 m/s for ships winds to 5.4 m/s for buoy winds. Scatterometer data, neglecting the ambiguity problem, have vector (not component) errors of order 2 m/s, smaller than the radiosonde errors. Considering that observations with potential ambiguity removal problems have been removed during the quality control, but that the radiosonde measurements should be given weight at least equal to that of scatterometer winds, we have chosen to set the scatterometer errors equal to the radiosonde errors.

2.4.2 *Data selection*

The analysis increment (the analysis minus the first guess at a particular point) is the weighted sum of the observation increments. The weights are found by solving a linear system, the size of which is equal to the number of observations used. If the same observations are used for several analysis points, the same matrix must be solved for each of these points. Consequently, the practical procedure employed by OI is to consider all analysis points in a box and all observations in a larger surrounding box, and to calculate the inverse of this matrix (*Lorenc*, 1981). (This inverse is also used in the OI quality check.) The box structure is illustrated in Fig. 10 for a location in the South Atlantic. A preset maximum number of observations is used. If too many data points are present in the surrounding box, only the closest data will be used. In extreme cases, the analysis box is subdivided, so that all the closest data to each analysis point can be used. As can be seen in the figure, the addition of scatterometer data greatly influences the data selection of other data. Clearly, using the scatterometer data at 50 km resolution causes the subdivision of the data box and overwhelms all other data types. The 100 km scatterometer data has an effect on data selection but only on data 500 km or more away from the edge of the analysis box. For such data, correlations with the locations in the analysis box will be small. Since it is not practical to increase the maximum number of observations used, and furthermore, since the resolution of our analyses is 200 km, we have used the 100 km resolution data in our experiments. It should be noted that the 100 km resolution data drops the first cell observed by the scatterometer. This reduces the data swath somewhat, but has the advantage of discarding data with known directional problems.

Preliminary experiments show that the scatterometer impact on the surface wind field analyses varies as the scatterometer estimated observational errors or data resolution is changed. These impacts are all very similar in location, shape and direction, differing mainly in magnitude. For example, impacts due to scatterometer data at 100 km resolution are similar, but of reduced magnitude when compared to impacts due to 50 km

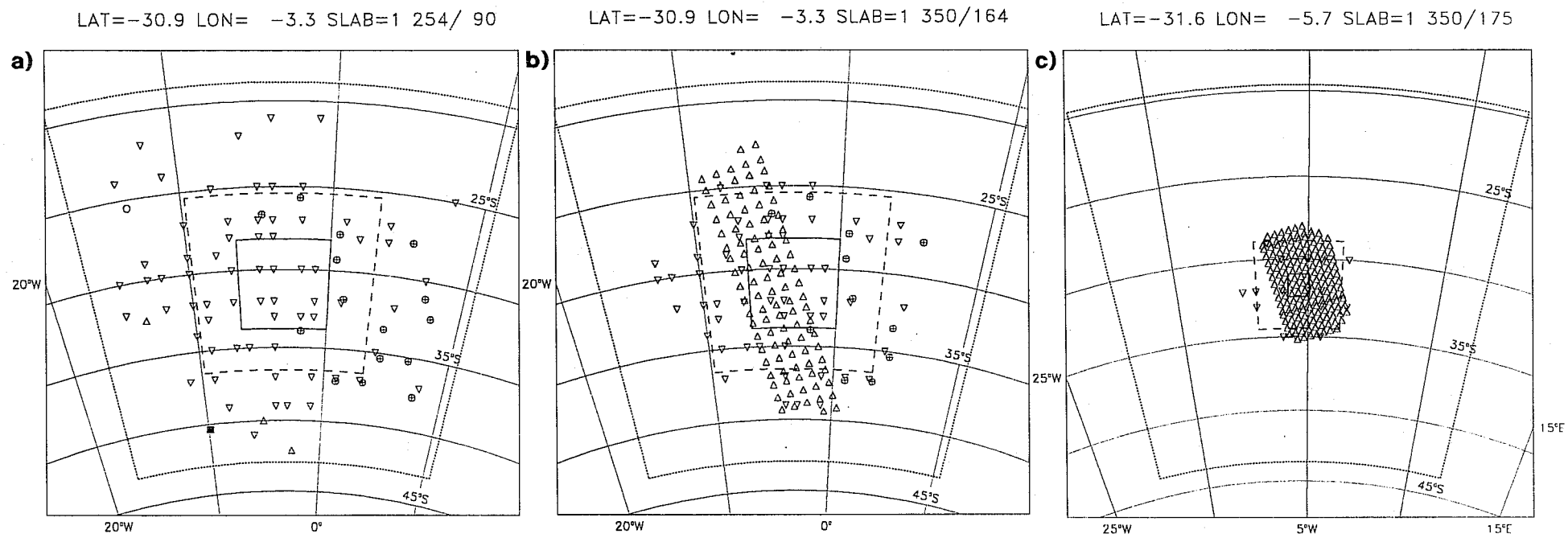

Fig. 10 Data selected for the analysis volume centered near 30°S, 4°W for (a) no scatterometer data, (b) 100 km resolution data and (c) 50 km resolution data, for 0000 GMT 6 November 1991. In each panel, the inner solid box is the analysis box, all data in the intermediate dashed box must be selected and only data within the largest dotted box is eligible for selection. Different symbols indicate different data types, as indicated in the legend.

resolution data. Since the additional scales in the 50 km resolution data should not be analyzed at the analysis resolution we are using, we should get very similar results whether the data are used at 50 or 100 km resolution. The differences we see are due to the fact that we are not using a proper model of the horizontal correlations of the scatterometer wind errors. The main effect of using proper horizontal correlations would be to reduce the weight of each datum - a similar effect can be obtained by thinning the data, or by increasing the magnitude of the estimated observational errors.

2.4.3 *Forecast error statistics*

In a general sense the ratio of the estimated prediction errors (i.e., the forecast error magnitudes) and the estimated observational errors determine how closely the analysis draws to the data. The forecast error correlations determine how the analysis spreads the influence of the data - horizontally, vertically and to the mass field. As we will see (Section 3.1), the wind analysis draws to the scatterometer data as expected, but the increments in the geopotential height field do not balance the wind increments geostrophically.

Since the data is restricted to relatively thin swaths and to the surface, spreading its influence in the horizontal and especially in vertical is important. The horizontal scale of the forecast error correlations is roughly 500 km. This effectively doubles the width of the zone affected by the scatterometer. Experiments by Atlas and others (*Baker et al.*, 1984; *Duffy and Atlas*, 1986; *Duffy et al.*, 1986; *Lenzen et al.*, 1992) show that the influence of scatterometer data must be extended in the vertical. In the next section it is seen that the vertical correlations used in OI are satisfactory in this regard with the increments at 700 mb being about half the 1000 mb increments.

The scatterometer data is also restricted to winds. Without balancing changes to the mass field, wind perturbations die away during the forecast. Evidently, geostrophy is not imposed rigidly in OI. There are three factors which contribute to deviations from geostrophic balance in the analysis increments. First, and most straightforwardly, the wind - height correlations include a geostrophy factor μ, which is +/- 0.90 in the extratropics and describes one half of a sine wave in a tropical band between 30°S and 30°N. Second, only the non-divergent part of the wind field is geostrophically coupled. This effectively multiplies μ by 0.90. Finally, the wind - wind correlations are incremented by 0.15 to account for the contribution of planetary scale wind forecast errors.

3. RESULTS

Generally, impacts are small. However, there are changes to the low level wind analysis at each synoptic time, especially in the Southern Ocean. The wind analysis impacts are greatly diminished during the 6 hour forecast, which generates the first guess for the next analysis. Impacts on the longer forecasts seem to be insignificant. The time averaged wind analysis differences shows that the first guess wind speeds are biased high compared to the scatterometer winds under conditions associated with higher than normal atmospheric stability. Further comparisons with ship winds suggest that there is some discrepancy in the boundary layer parametrization in the model under stable conditions.

In order to illustrate and explain the impacts we observe, we will focus on particular meteorological features for which the SCATT - CONTROL differences are relatively large or easy to see. However, in absolute terms these differences are neither large nor easy to see. We have examined differences in other features, and the cases described here are representative, except, in some cases, for their magnitude, of analogous differences at other times and locations.

3.1 Analysis Impacts

Here we examine the data impact by considering SCATT - CONTROL analysis and forecast differences and examining the fit of the SCATT and CONTROL analyses to the data. This shows the manner in which the analysis fits the data, both the degree to which it draws to the data and the extent to which the data influence is extended in the vertical and to the mass field. We do not present any analysis fields here, but some are shown in the next section, as the initial conditions for the forecasts.

The results presented in this section are for 1200 GMT 28 and 31 December, the starting times of two of our forecasts. The analysis differences seen are principally due to the scatterometer data used at the analysis time. Throughout the experiment analysis differences tend to decay during the 6 hour forecasts which generate the first guess. There are some exceptions to this. During the first 3 days of the experiment a small change to a ridge south of Australia, develops and persists. During this period, it is the dominant difference. The structure of this differences is very barotropic, with surface wind increments of 12 m/s, surface pressure increments of 10 mb and 500 mb geopotential height increments of 60 meters. This feature appears to be unrepresentative. Once established it does not seem to evolve, other than to be advected by the mean flow. After a few days it dissipates without having had a noticeable impact on the subsequent evolution of the analysis and forecast fields.

The scatterometer data used in the SCATT analysis at 1200 GMT 28 December are shown in Fig. 11. In the figure, the tracks running NE to SW (SE to NW) are descending (ascending) orbits. For example, in the Atlantic, the satellite is travelling from North to South and the inner edge of these swaths are on the east. Since CREO does not produce winds under a variety of conditions (Section 2.2), the wind data

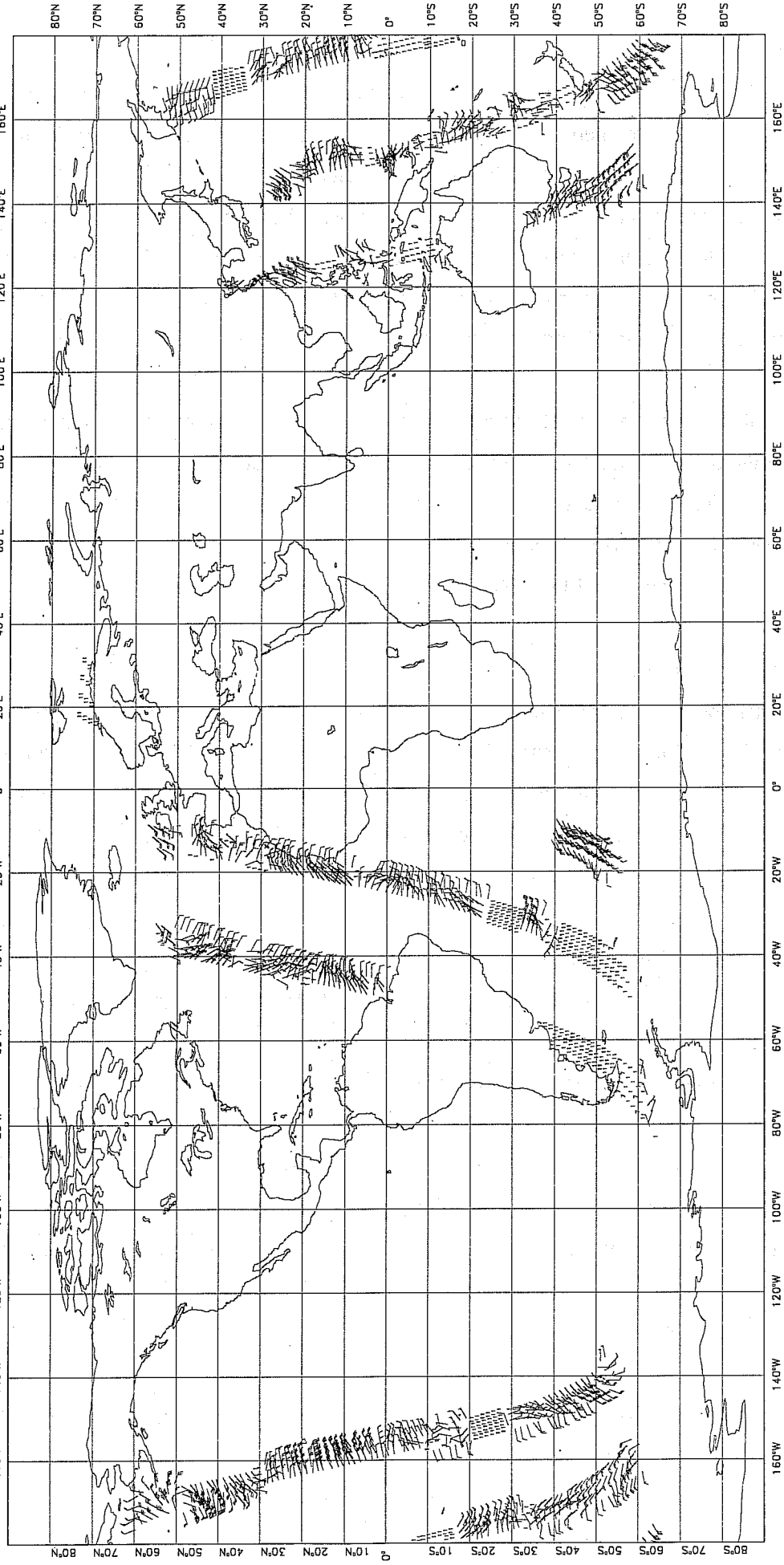

Fig. 11 CREO scatterometer winds for 1200 GMT 28 December. From the SCATT experiment.

coverage is far from continuous. The wind analysis differences in the lowest model layer reflect this data coverage (Fig. 12). The circulation feature near 65°S 130°E is that discussed above. Differences in regions of no scatterometer data, e.g. the Indian Ocean, are due to data at previous times. The rapidity with which the differences in the wind field decay, is evident here.

The decay of the wind analysis differences is due to the 6 hour forecast. Fig. 13 shows the cycle in SCATT - CONTROL differences of first guess, analysis, initialized analysis and first guess again, for the area south of New Zealand, where there is a patch of scatterometer winds of up to 35 knots. The initialization has virtually no effect on the wind field impact, and increases the mass field impact. The rightmost panels in this figure shows that the first guess forecast advects these differences towards the east and reduces the amplitude of the wind analysis differences by a factor of three.

For this same area, the extension of the data in the vertical and to the mass field is shown in Fig. 14. In the vertical the differences decay with increasing height, and are barotropic (i.e., they are straight up and down, with no tilt). The maximum vector wind difference of 7 m/s at 1000 mb, decays to 5 m/s at 850 and 3 m/s at 700 mb. In the mass field, the maximum surface pressure difference is 2 mb and the maximum geopotential height difference is less than 20 m near the surface, decreasing to 10 m at 700 mb.

The analysis fits the scatterometer wind data very well. Fig. 15 shows the SCATT statistics for the data passing the quality control at 1200 GMT 31 December. (We have already considered the data failing the quality control in Section 2.3) There is a tendency to fit the u component slightly better than the v component here as well for other analysis times. In terms of rms wind speed and direction the analysis fits the data to about 1.2 m/s and 15° (Fig. 16). The fact that the SCATT analysis fits the data so well is due to the fact that the estimated observational errors are small compared to the estimated prediction errors and that the data are horizontally consistent. If we examine similar fits for the CONTROL experiment we find that the scatterometer data are not fit so well. In this case, the fit is the same before and after the analysis and the same as the fit before the analysis in the SCATT experiment (Fig. 17).

3.2 Forecast Impacts

The forecast impact is easily summarized by the time evolution of anomaly correlation coefficients and rms errors. Since the analysis impacts are small for mass and tend to decay during the 6 hour forecast for winds, it is not surprising that the forecast impacts are small. If we look at individual features of the forecast, some are improved significantly and some are deteriorated significantly in SCATT compared to CONTROL. The anomaly correlation coefficient scores and rms errors average over many meteorological features and generally show no impact except in the Southern Hemisphere. In the Southern Hemisphere out of four forecasts we find one positive, two neutral and one negative impact due to scatterometer data. When averaged over the four cases, there is essentially no impact. We are unable to trace the forecast impacts on

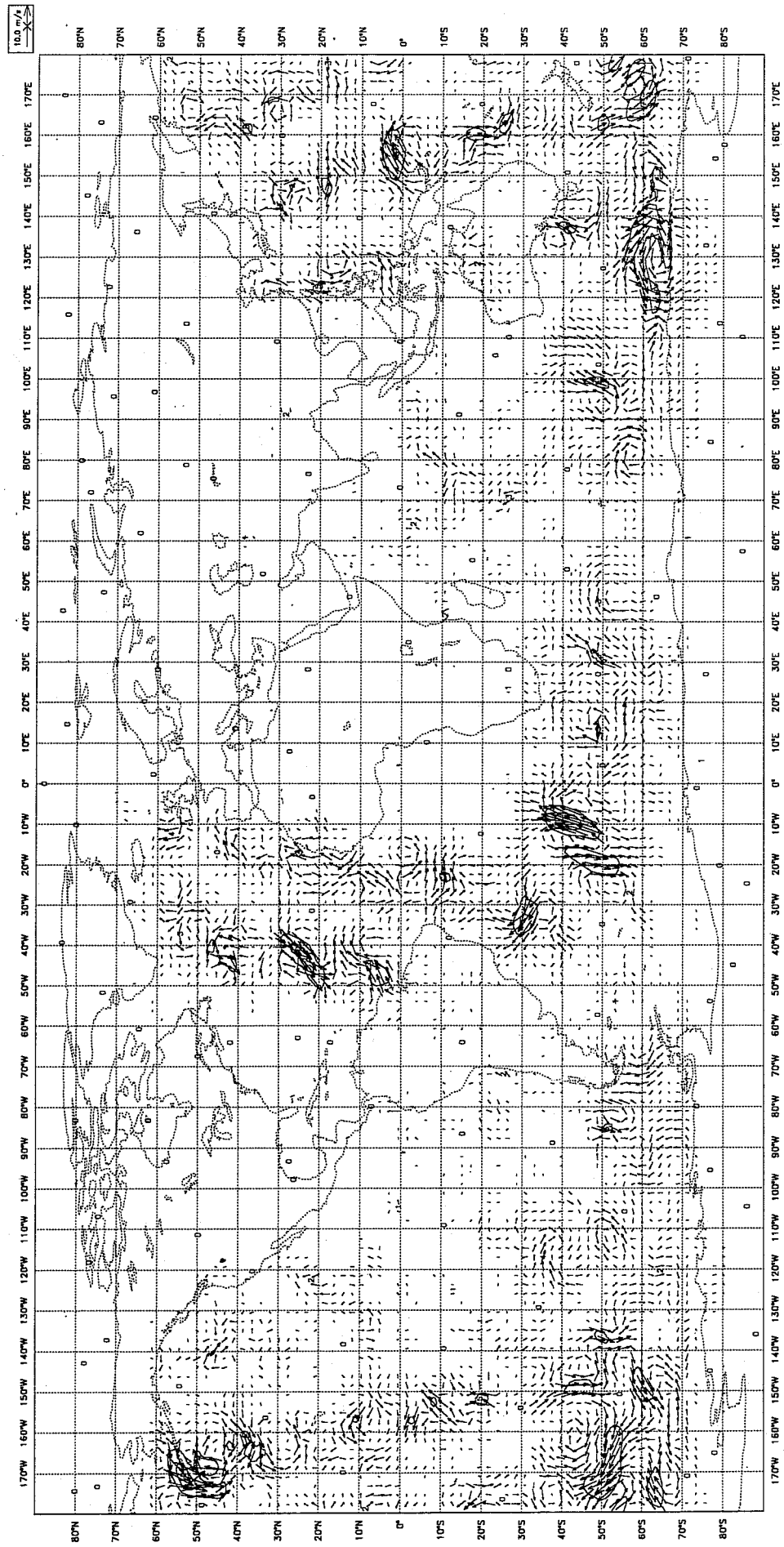

Fig. 12 Difference of the analyzed wind field, SCATT - CONTROL, in the lowest model layer, for 1200 GMT 28 December

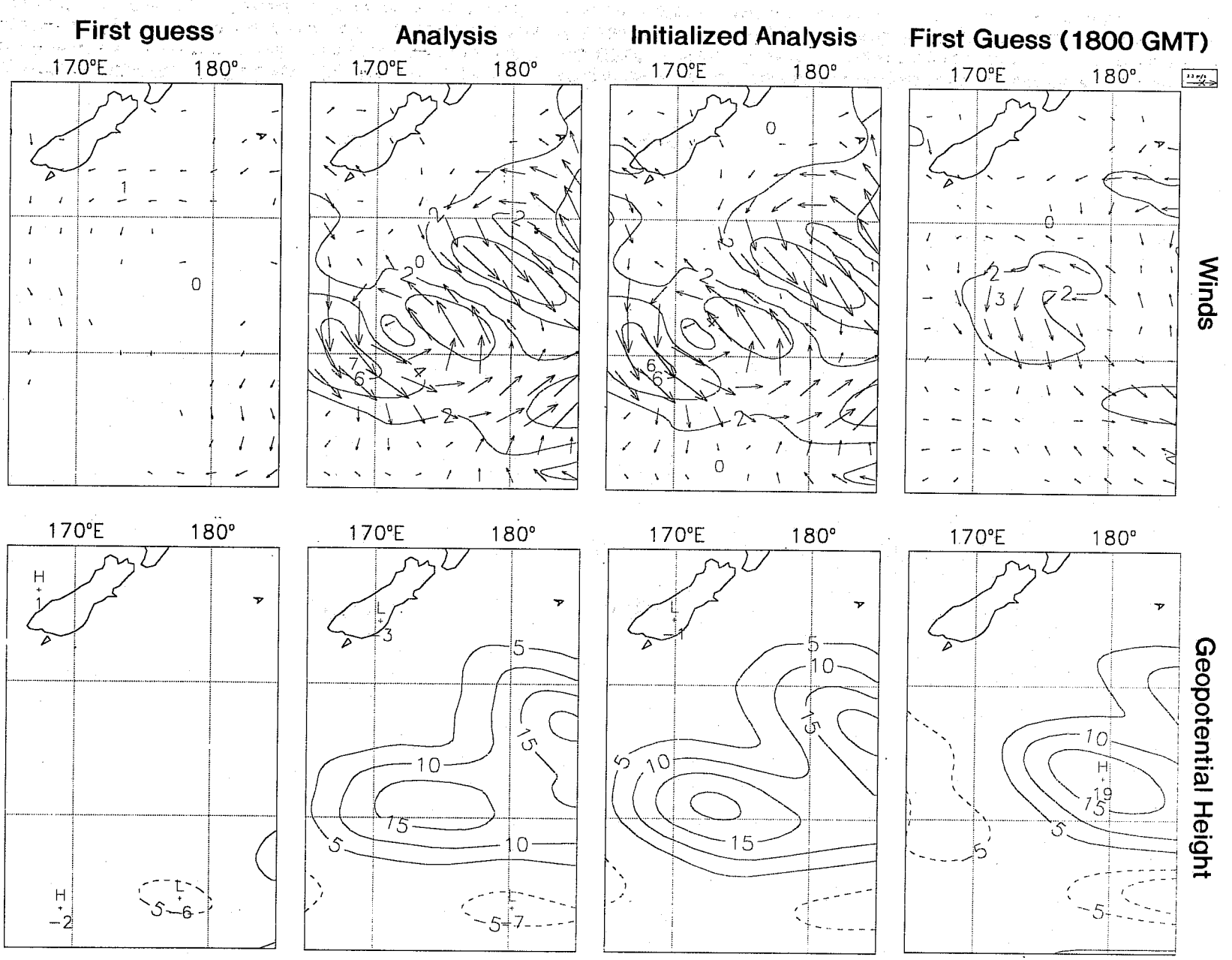

Fig. 13 Difference (SCATT - CONTROL) of 1000 mb wind (top) and geopotential height (bottom) for (from left to right) the first guess, analysis and initialized analysis at 1200 GMT and the first guess again at 1800 GMT, all for 28 December.

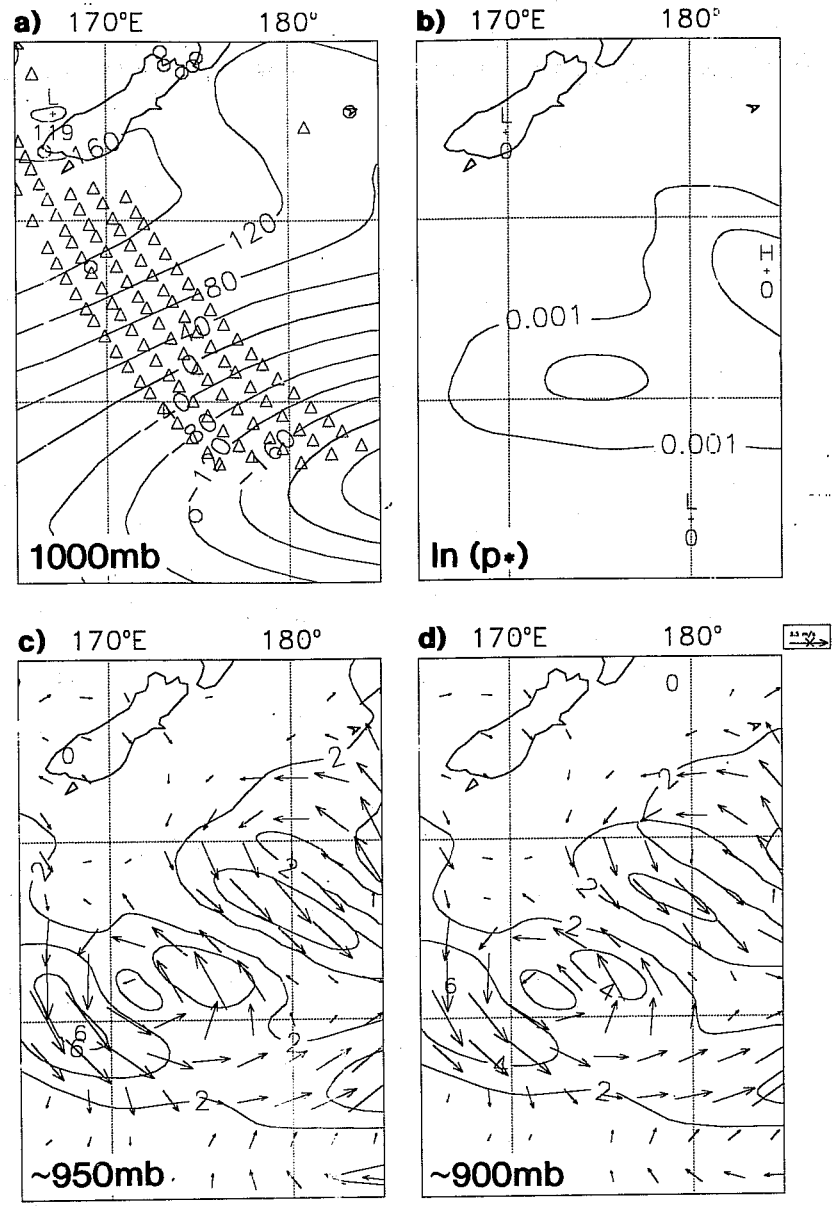

Fig. 14 Data spreading at 1200 GMT 28 December. The first panel (a) shows the 1000 mb geopotential height SCATT analysis (40 m contour interval) and the locations of CREO scatterometer winds used in that analysis. The other panels are SCATT - CONTROL analysis differences for log and surface pressure (~1 mb contour interval) (b); wind at model levels 17 (c) and 16 (d) and at mandatory pressure levels 1000, 850, 700 and 500 mb (e-h) (2 m/s contour interval); and geopotential height at these mandatory pressure levels (i-l) (5 m contour interval). Differences in log of surface pressure multiplied by 1000 are very nearly equal to differences in surface pressure in mb. Model levels 17 and 16 correspond roughly to mandatory pressure levels of 950 and 900 mb.

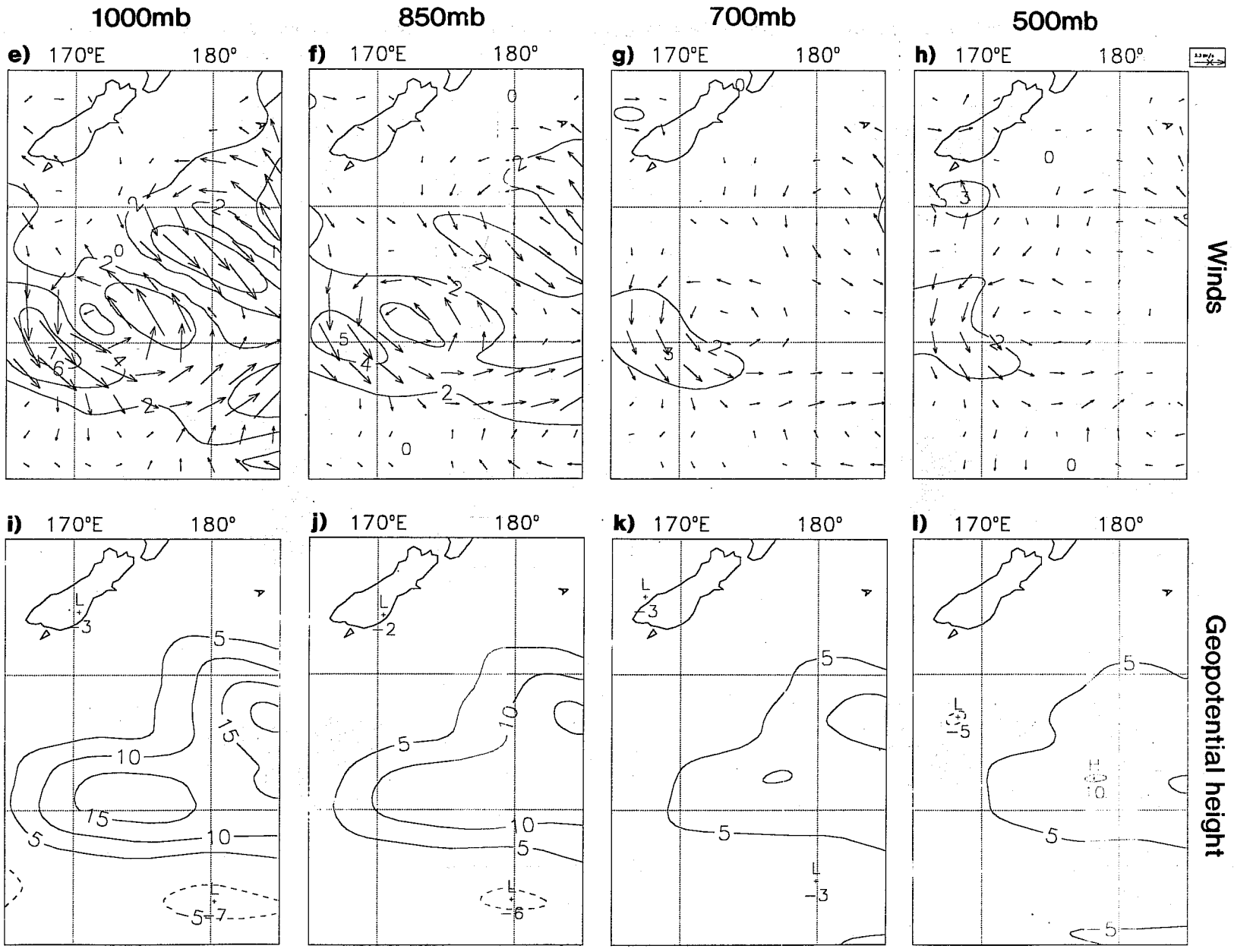

Fig. 14 continued

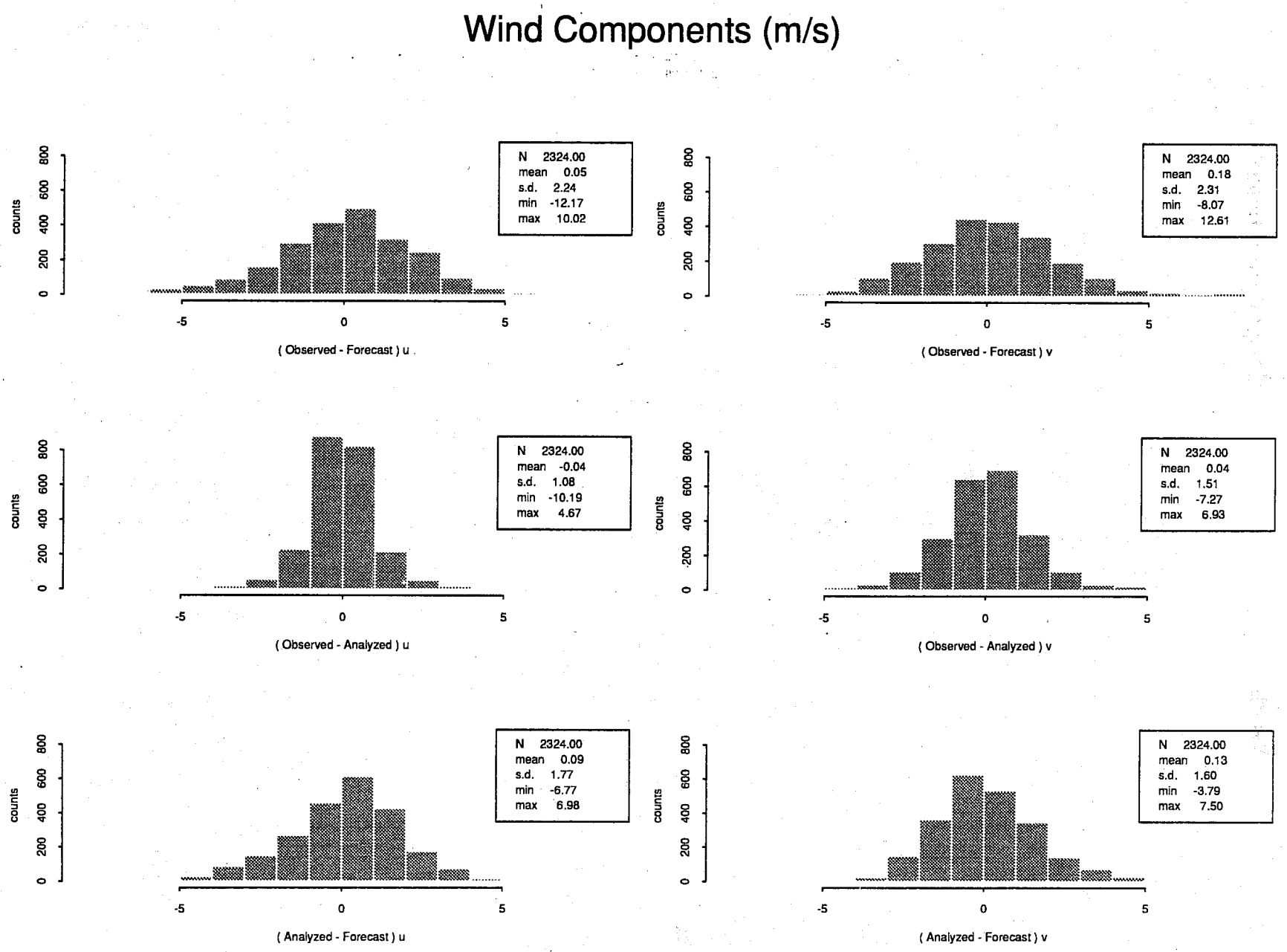

Fig. 15 Histograms of increments for *u* and *v* wind components for the SCATT experiment analysis of 1200 GMT 31 December.

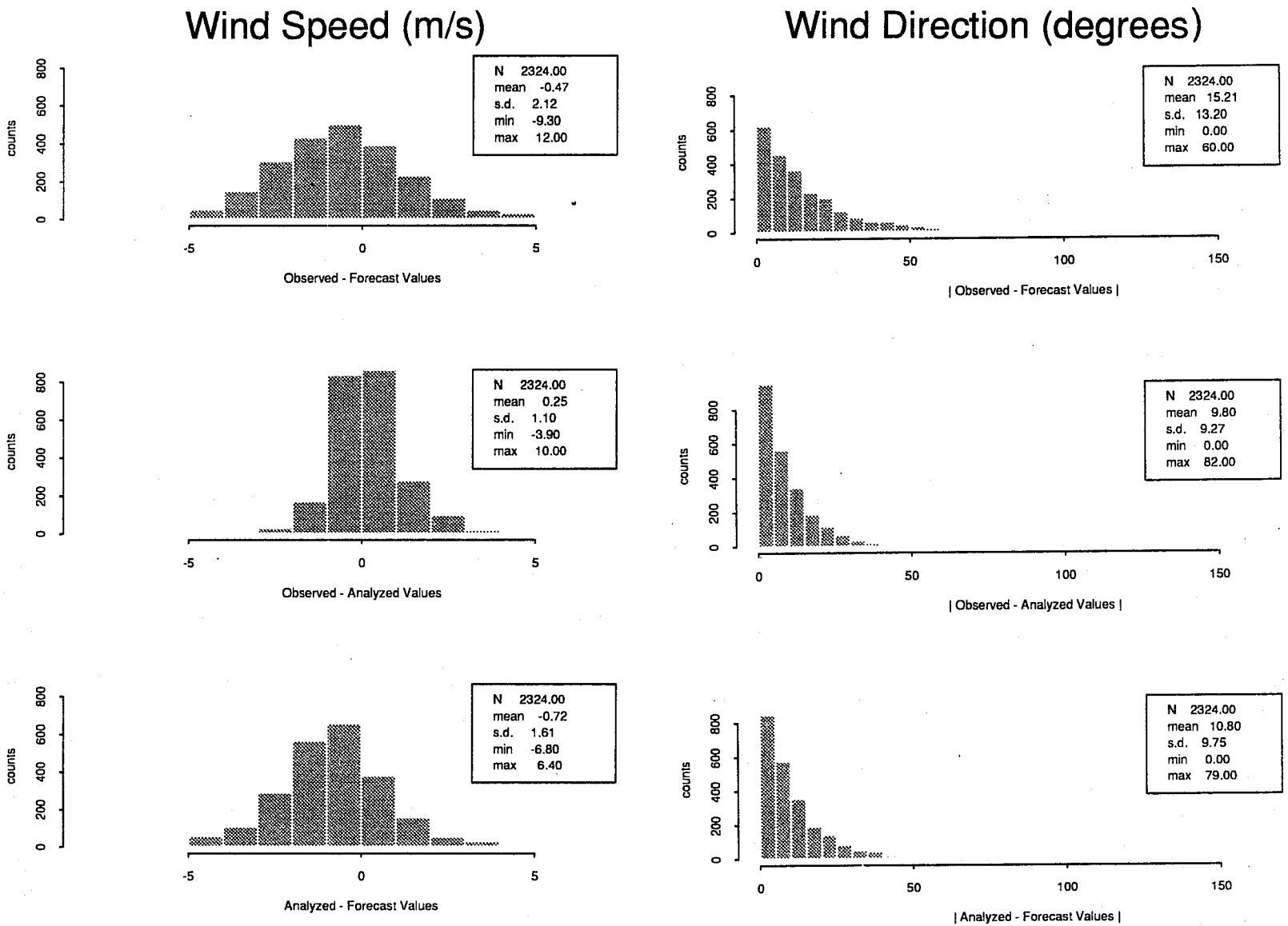

Fig. 16 As in Fig. 15 for wind speed and direction.

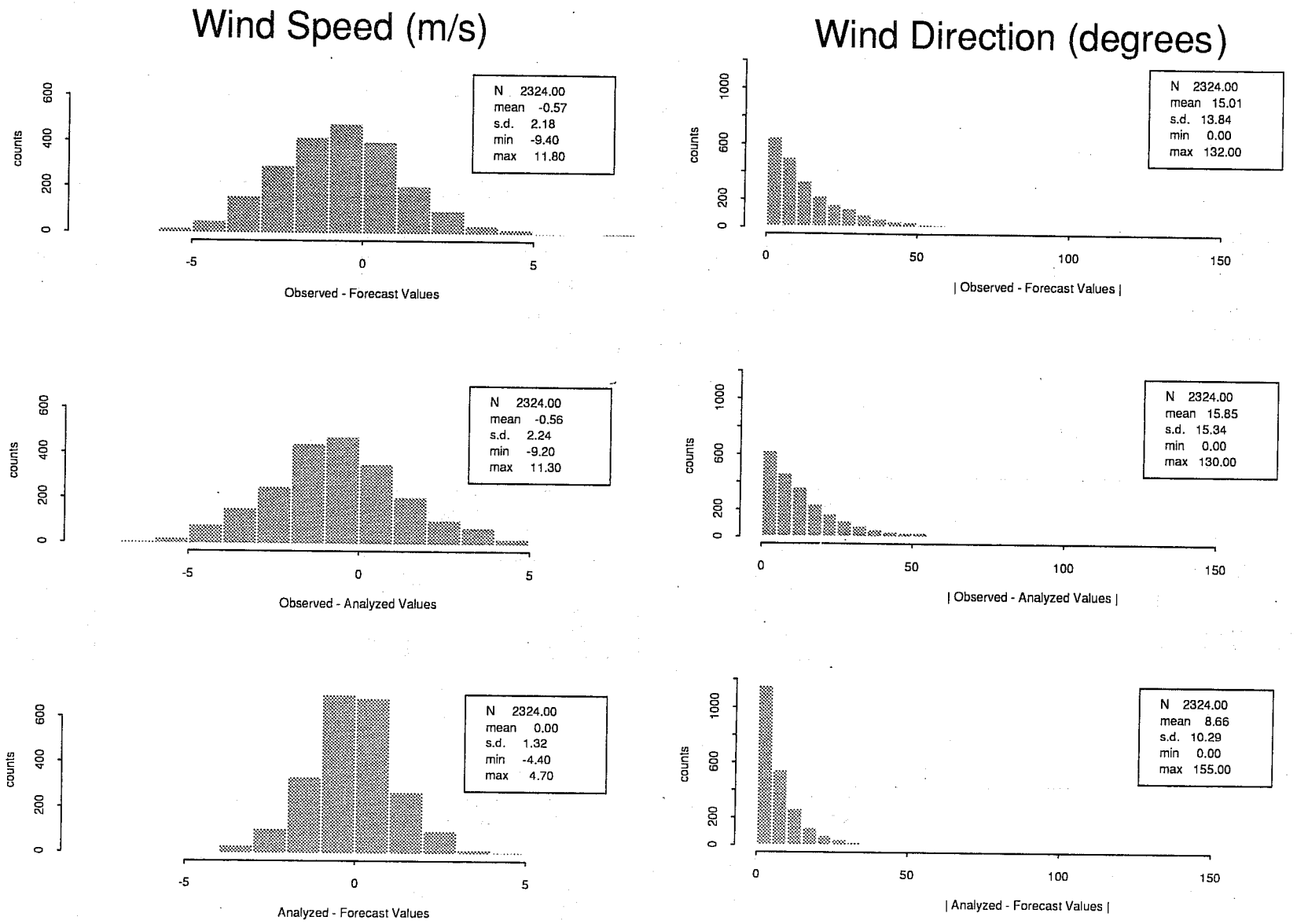

Fig. 17 As in Fig. 16 for the CONTROL experiment.

individual features back to particular scatterometer data. Although the scatterometer data must be the ultimate cause of differences in the forecasts, it appears that the differences arise from small quasi-random perturbation which grow in the guess forecasts in the data sparse Southern Hemisphere.

The ensemble average anomaly correlation coefficients scores for geopotential height and rms errors for winds for the Northern Hemisphere (20°N to 90°N), Southern Hemisphere (20°S to 90°S) and tropics (20°S to 20°S) show extremely small impacts (Fig. 18). On a case by case basis, the impacts are small as well, except in the Southern Hemisphere. The Southern Hemisphere scores for 1000 mb geopotential height are shown in Fig. 19. The impact on the scores for wind and at other levels parallel those seen in Fig. 19.

We will consider the evolution of four features in three of the forecasts in an attempt to identify particular impacts with particular scatterometer data. First we consider two features in the forecast of 0000 GMT 2 January. The clearest impacts on the analyzed mass field are seen for these features. Then for the cases of 1200 GMT 28 and 31 December, which are respectively, the cases of negative and positive impact, we study two features in the forecasts which stand out in the difference fields.

At the start of the forecasts at 0000 GMT 2 January, all three analyses (the operational analysis, the SCATT analysis and the CONTROL analysis) have a 1000 mb low near 20°E, 60°S (Fig. 20). The 1000 mb surface is 30 m lower in the SCATT analysis. At 60°S, 150°W there is another low. It is strongest in the operational analysis and weakest in the SCATT analysis. The CONTROL analysis positions this low considerably south of the others. These differences can be traced back in time in the analyses (Fig. 21) and forward in time in the subsequent forecast (Fig. 20). At 24 h, both of these features are better forecast in the SCATT experiment, but by 48 h these features have dissipated in the operational analysis and are poorly forecast by both SCATT and CONTROL. At the same time, some of the nearby features are better forecast by CONTROL (e.g. the secondary low at 140°W, 60°S).

For the case of 1200 GMT 28 December, the five day SCATT forecast has a very distinct low pressure system, at about (10°E, 45°S), which is not present in the CONTROL forecast or the operational analysis (Fig. 22). It is very unlikely that the SCATT forecast is correct in this regard. First, this feature can be traced backwards in time only to day 2 of the forecasts (Fig. 23). Second, there is no clear evidence for such a system in the time evolution of surface pressure at Gough Island (9.88°W, 40.35°S). Finally, the visible image, from the geostationary satellite METEOSAT, for this time and location is clear.

For the case of 1200 GMT 31 December, the three day forecasts have misplaced a ridge, present in the operational analysis of 1200 GMT 3 January, running SW - NE centered around 15°E, 50°S (Fig. 24). In the SCATT forecast this ridge is approximately at 27°E, while in the CONTROL it is at 33°E. At this time the difference in this feature dominates the SCATT - CONTROL difference (Fig. 25). This feature can be

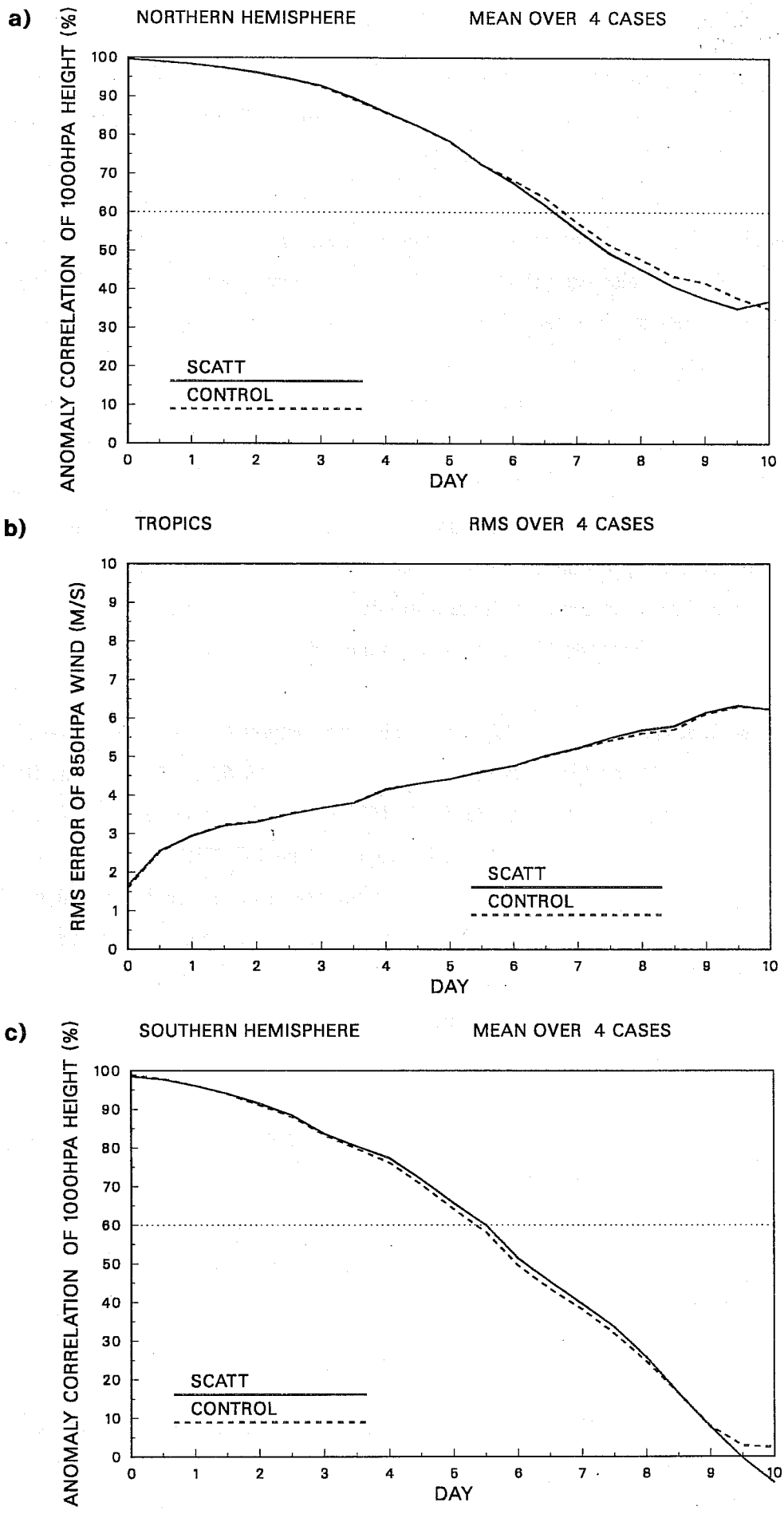

Fig. 18 Time evolution of ensemble mean forecast scores for SCATT (solid) and CONTROL (dashed) for (a) Northern Hemisphere 1000 mb geopotential height, (b) Tropical 850 mb wind and (c) Southern Hemisphere 1000 mb geopotential height. Note that (a) and (c) shows anomaly correlation coefficients and (b) shows rms errors.

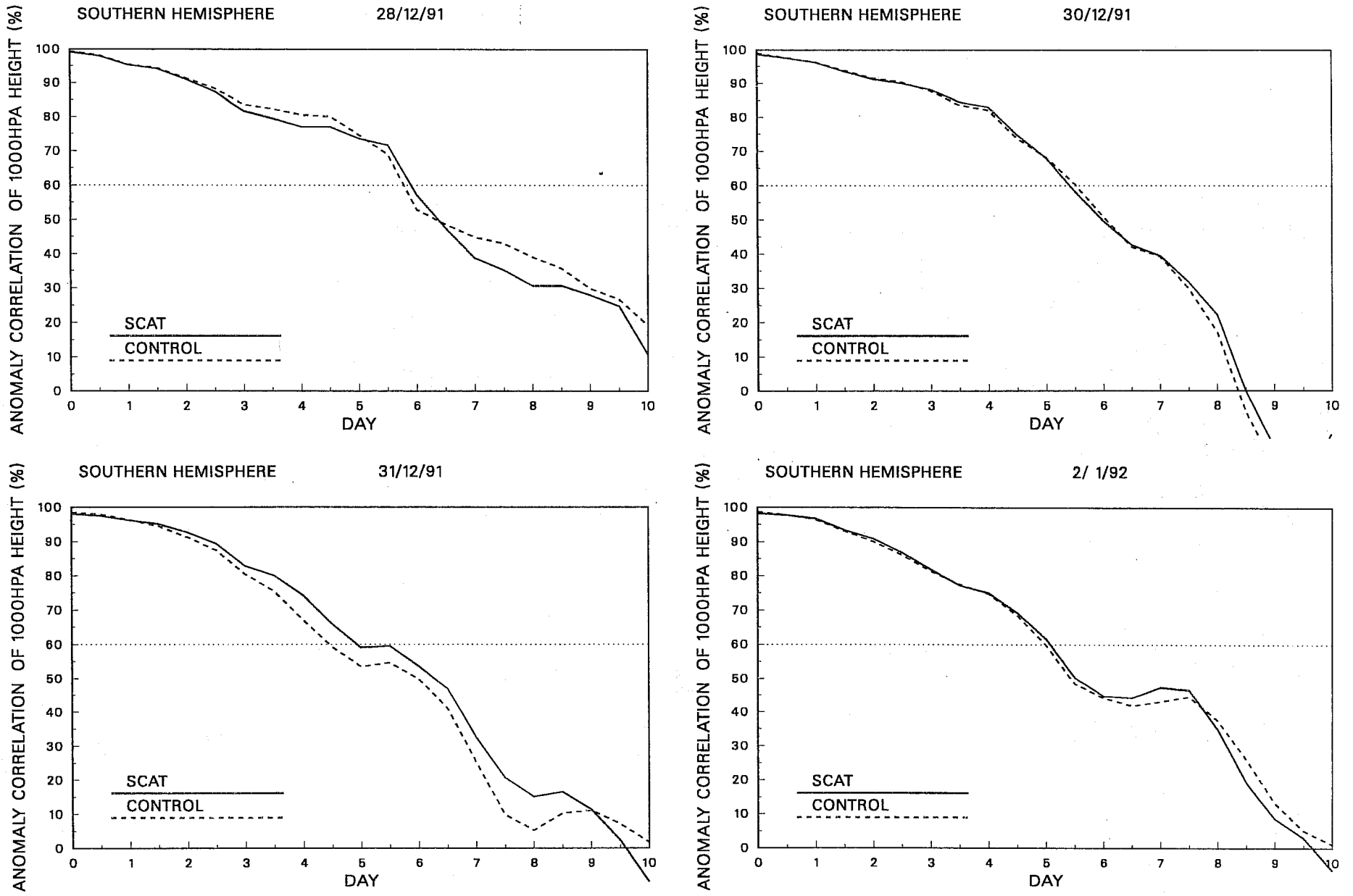

Fig. 19 Time evolution of anomaly correlation coefficients for Southern Hemisphere 1000 mb geopotential height for the four forecasts, for SCATT (solid) and CONTROL (dashed).

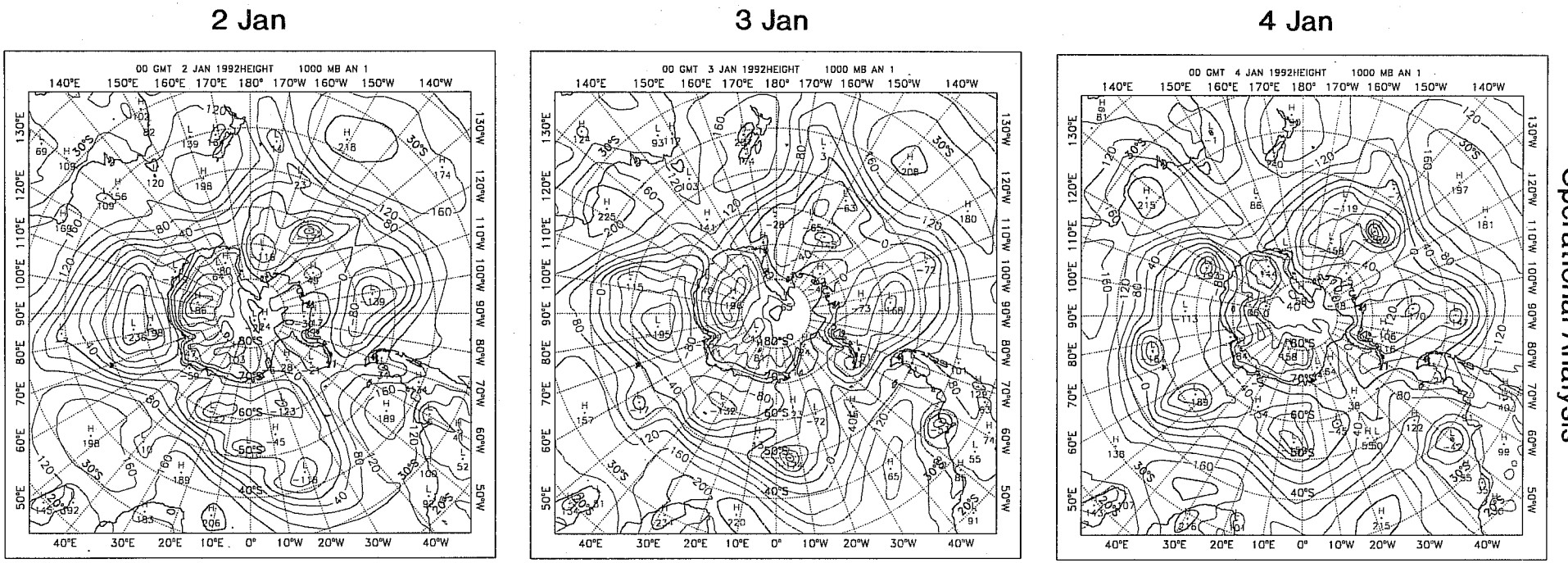

Fig. 20 Analyses and forecasts of 1000 mb geopotential height for the Southern Hemisphere for the case of 0000 GMT 2 January. From left to right time advances from 0000 GMT 2 January to 0000 GMT 3 January to 0000 GMT 4 January. The top row is the operational analyses, the second row is the SCATT forecast and the third row is the CONTROL forecast. (40 m contour interval.) Note that the operational analyses at the intermediate times of 1200 GMT on January 2 and 3 are presented on succeeding figures.

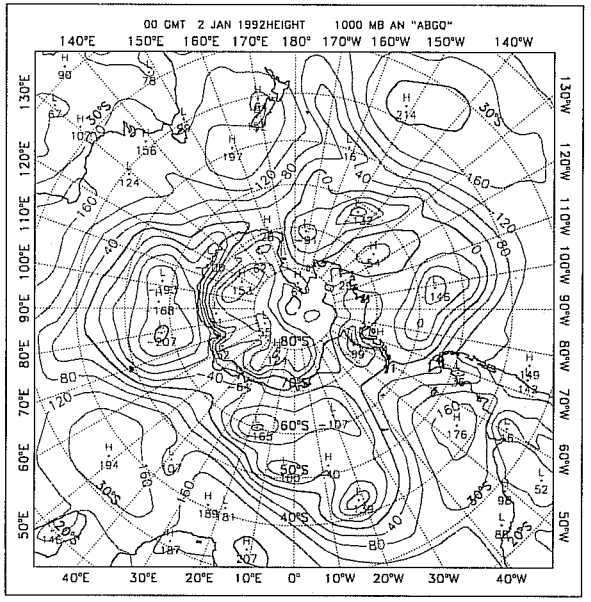

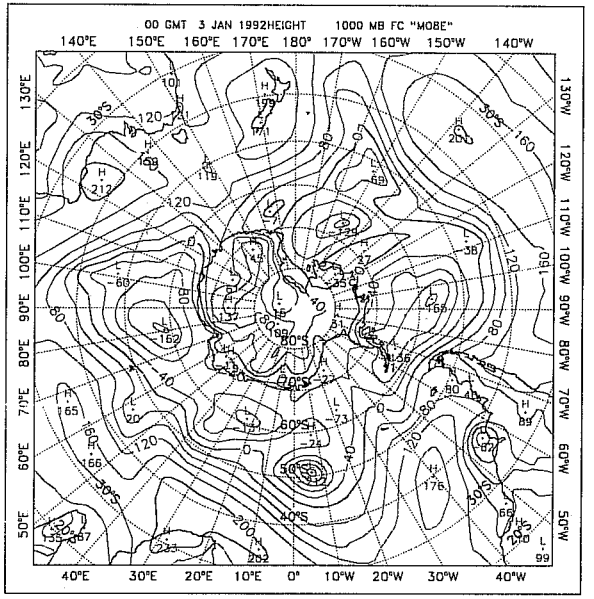

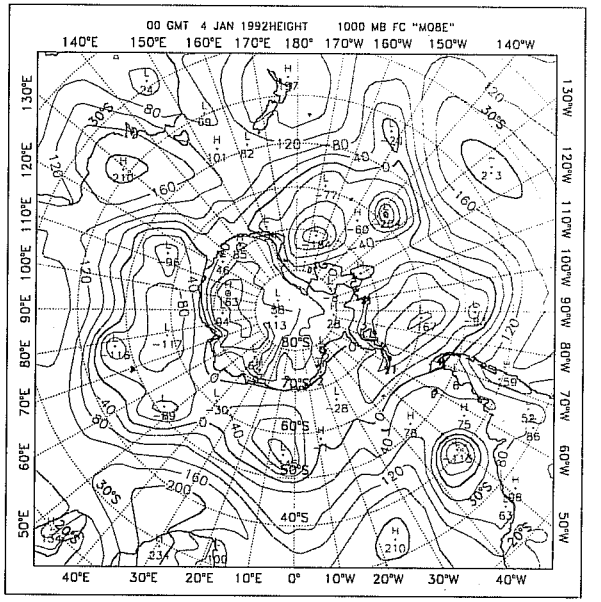

SCATT

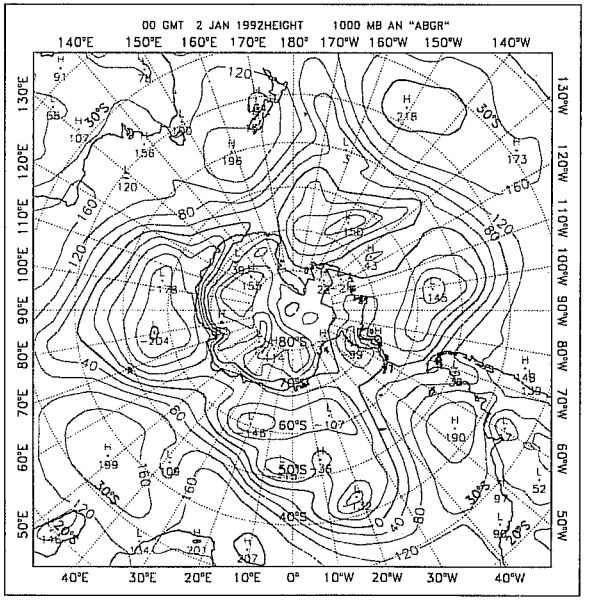

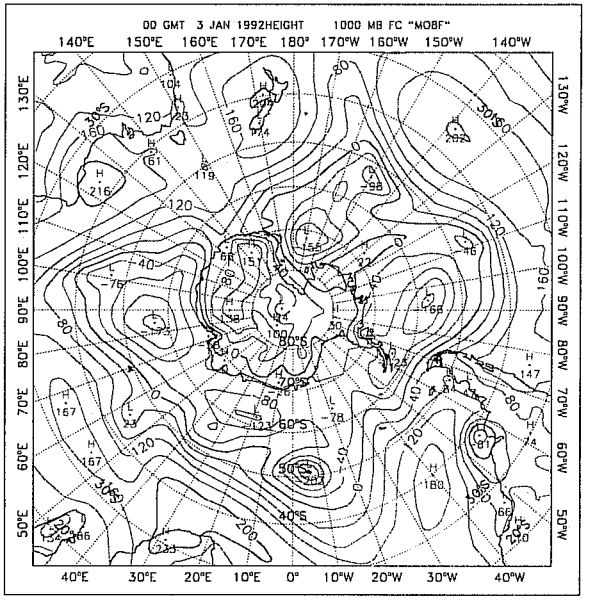

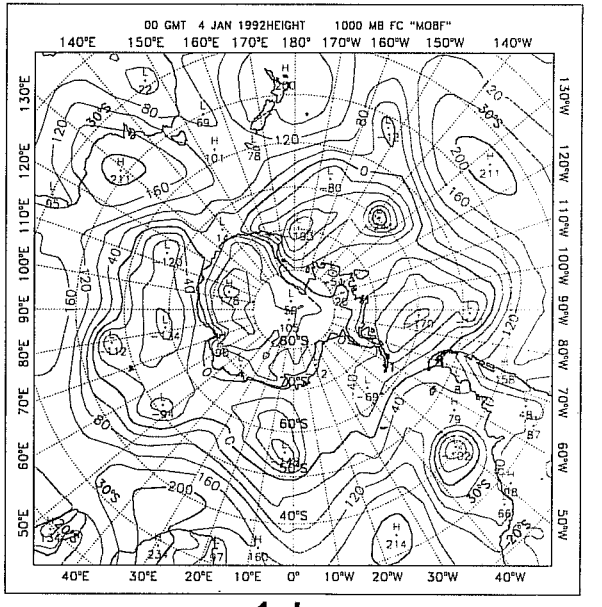

CONTROL

2 Jan 3 Jan 4 Jan

Fig. 20 (cont)

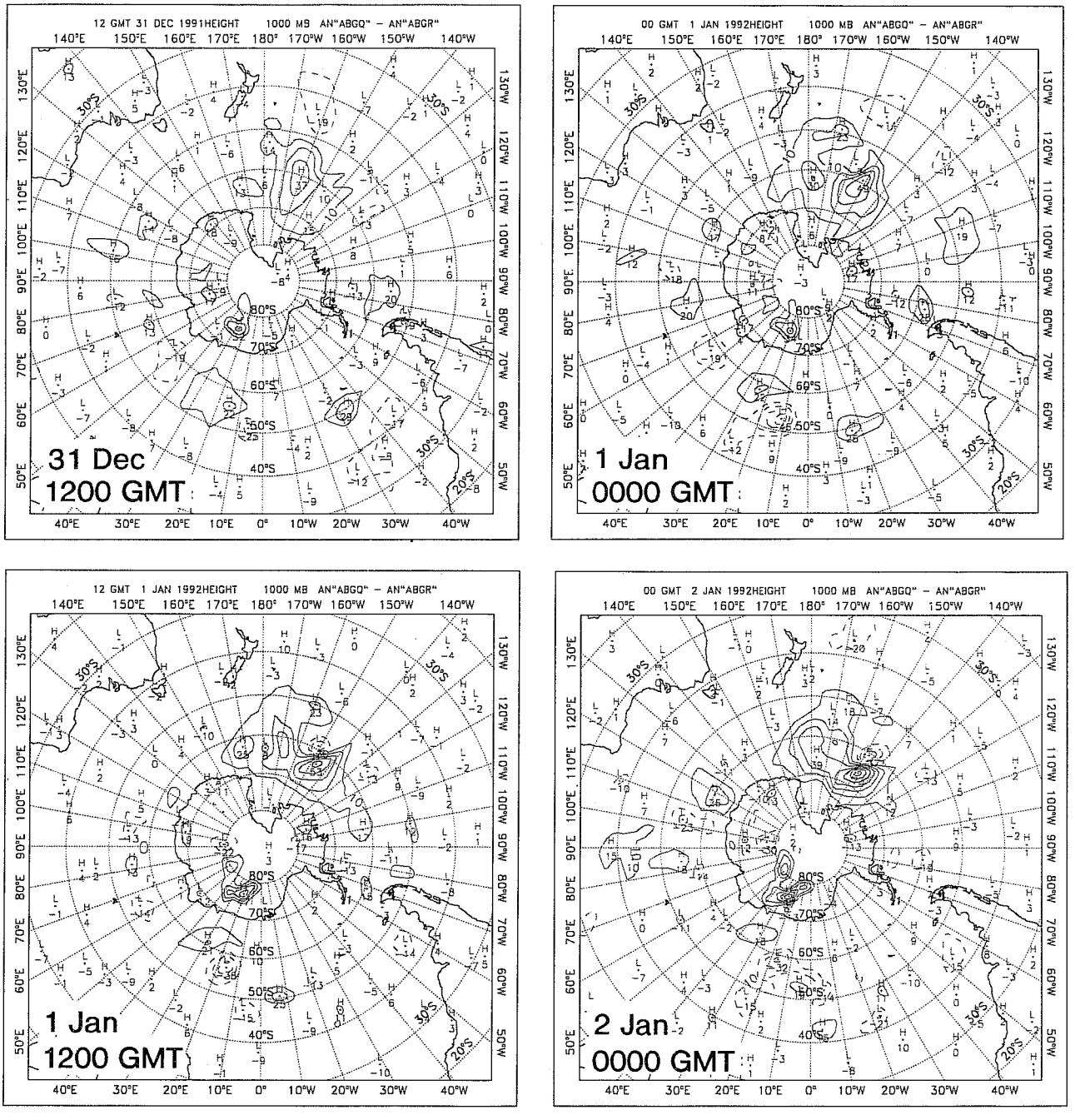

Fig. 21 SCATT - CONTROL analysis differences for 1000 mb geopotential height for the Southern Hemisphere for 1200 GMT 31 December, 0000 and 1200 GMT 1 January and 0000 GMT 2 January. (10 m contour interval.)

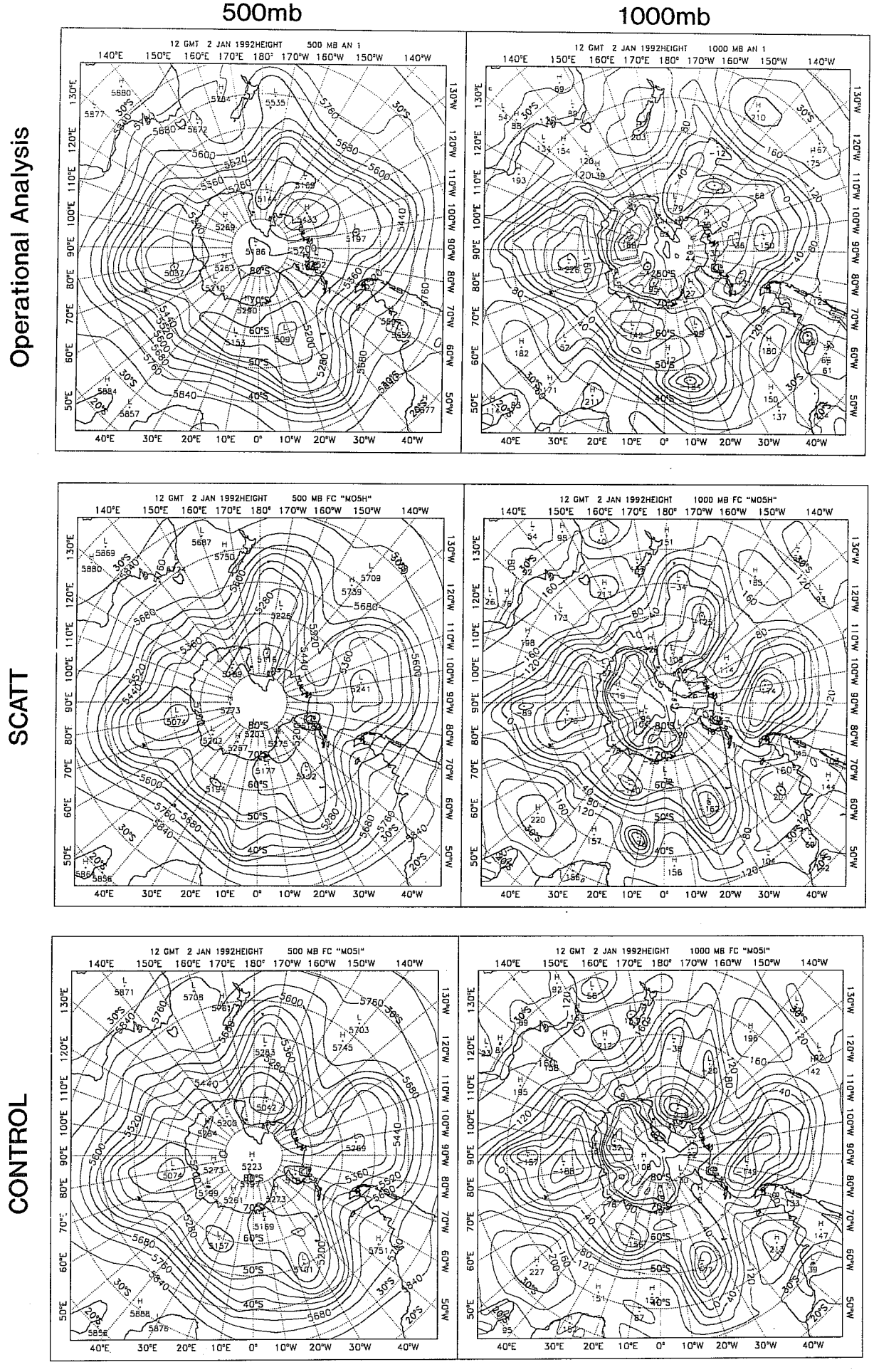

Fig. 22 Forecasts and analyses valid at 1200 GMT 2 January for the Southern Hemisphere for 500 mb (left) and 1000 mb (right) geopotential height for (from top to bottom) the operational analysis and the 120 h SCATT and CONTROL forecasts. (80 and 40 m contour intervals.)

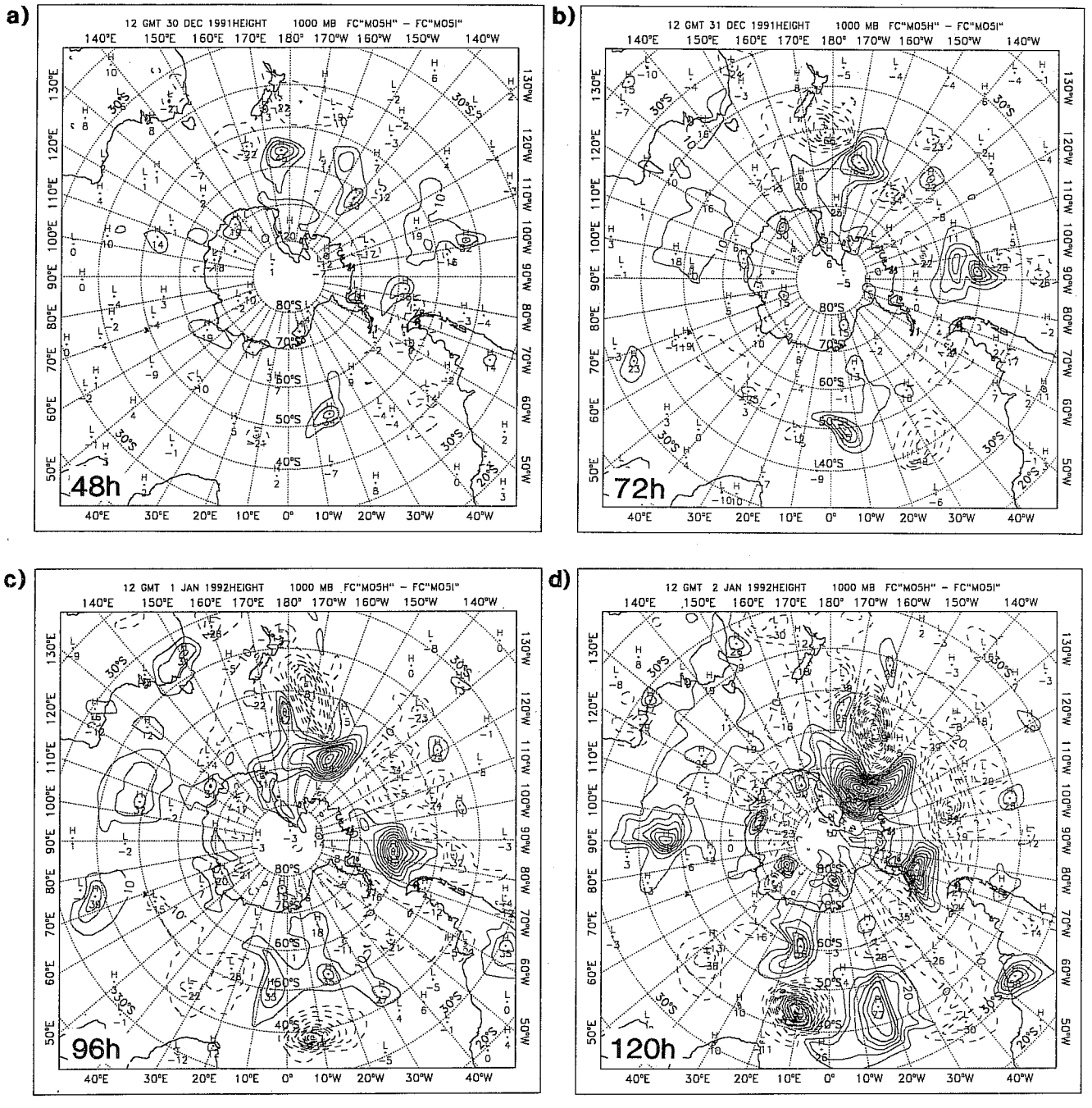

Fig. 23 SCATT - CONTROL forecast differences for the Southern Hemisphere 1000 mb geopotential height for the forecast beginning 1200 GMT 28 December for forecasts of (a) 48 h, (b) 72 h, (c) 96 h and (d) 120 h. (10 m contour interval.) Note that (d) is the difference of the bottom right 2 panels of Fig. 22.

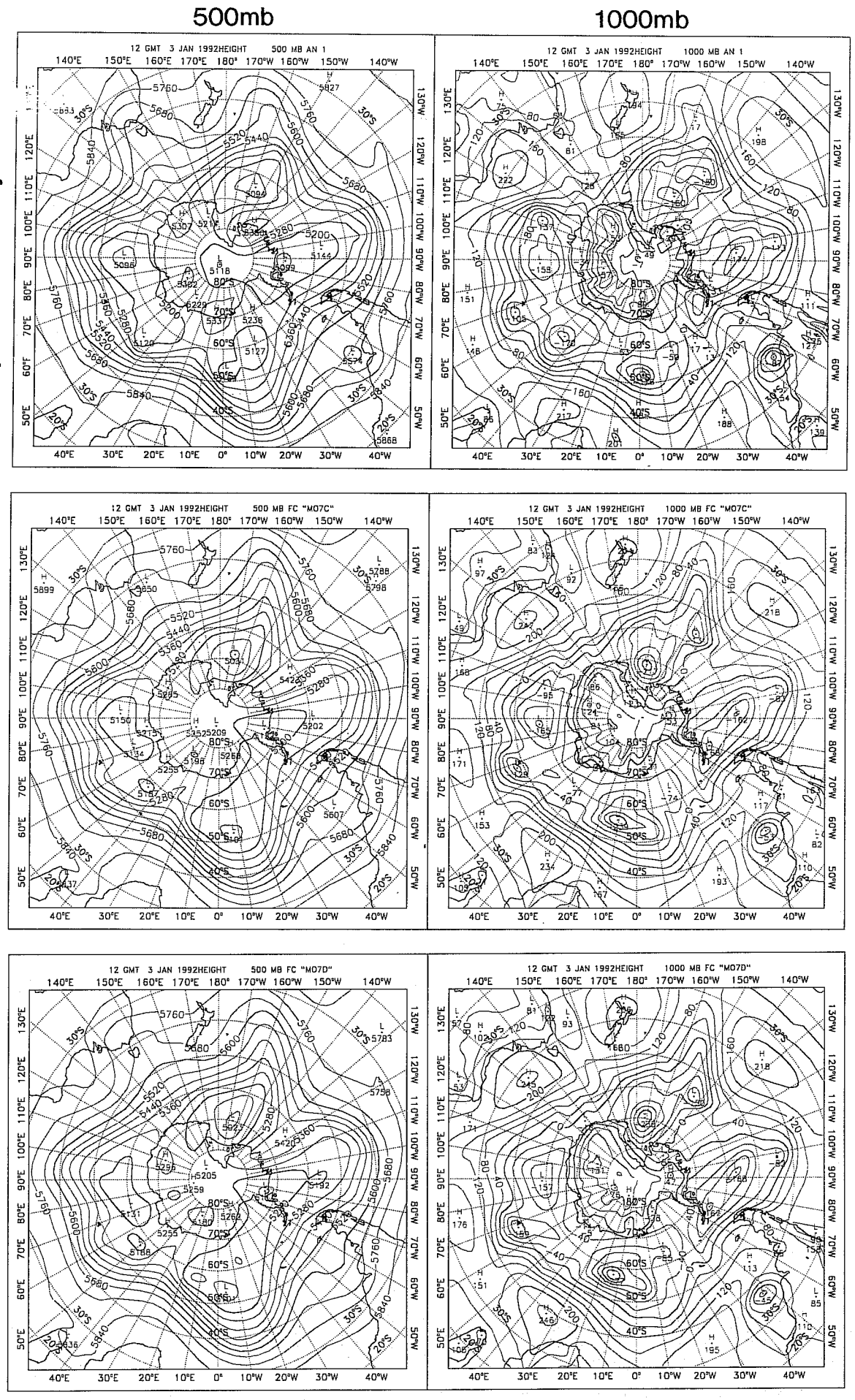

Fig. 24 Forecasts and analyses valid at 1200 GMT 3 January for the Southern Hemisphere for 500 mb (left) and 1000 mb (right) geopotential height for (from top to bottom) the operational analysis and the 72 h SCATT and CONTROL forecasts. (80 and 40 m contour intervals.)

traced back to the analysis time in the SCATT - CONTROL difference maps, but only to a very small 1000 mb geopotential height perturbation. This perturbation is between two swaths of scatterometer data used in the analysis (Fig. 26). However it was already present in the differences of the first guess. In fact it can be traced back an additional 24 hours in the pressure field analysis differences (Fig. 27).

3.3 An inconsistency between the scatterometer data and the ECMWF first guess

We examined differences in the analyzed wind fields averaged over the last 5 days (i.e. the last 21 analyses) of the experiment. The largest differences are O(1-2 m/s) and are found close to the surface and primarily in the Southern Hemisphere. The averaged CONTROL and SCATT - CONTROL lowest layer (32 m) wind fields are shown in Fig. 28. The main differences correspond to the scatterometer decelerating the flow. Further this effect is largest when the flow is from the NW. This suggests that the scatterometer winds are slow when there is warm air advection and increasing stability, or that the CONTROL Southern Hemisphere analysis is fast under these conditions.

With regard to the scatterometer data, a potential explanation of these differences lies in the method by which OI compares the scatterometer observed wind to the first guess wind. Scatterometer wind data are usually considered to be neutral stability winds at some reference height, 10 m for ERS1. In our experiments the first guess wind is the forecast model wind at 10 m which includes stability effects. Under stable conditions, the model 10 m wind speed will be larger than the neutral wind speed, and the scatterometer observations will appear to be biased low relative to the forecast. This is just what we have seen. However, the effect of correcting the model 10 m winds to neutral conditions would be small (O .1 - .2 m/s) (Fig. 29). This figure is calculated using the boundary layer formulation of the forecast model (*Louis*, 1979).

Further evidence for the possibility that the Southern Hemisphere CONTROL analysis is too fast under stable conditions is seen in Fig. 30. Two different comparisons are made here. The first panel compares the difference in scatterometer and CONTROL analysis wind speed with the northward component of the CONTROL analysis wind. The data sample used in this panel is for $v > 5$ m/s in the Northern Hemisphere (20°N to 90°N) for the last 48 hours (i.e. last 8 analysis periods) of the experiment. Increasing v is in turn associated with increasing stability. (Unfortunately, the diagnostics files saved from our experiment, do not include direct stability measures.) Analogous plots for the entire globe show a similar relationship. The second panel compares the difference in ship and operational first guess wind speed with the northward component of the operational first guess wind. The data sample is for the operational first guess $v > 5$ m/s in the Northern Hemisphere for the period 1200 GMT 26 - 31 December. The correspondence between the two panels is striking. It appears that in cases of warm air advection, the first guess is too fast. In the Northern Hemisphere for SCATT and CONTROL and in the Southern Hemisphere for SCATT, there is sufficient data to correct the analysis in these cases. In the Southern Hemisphere CONTROL experiment,

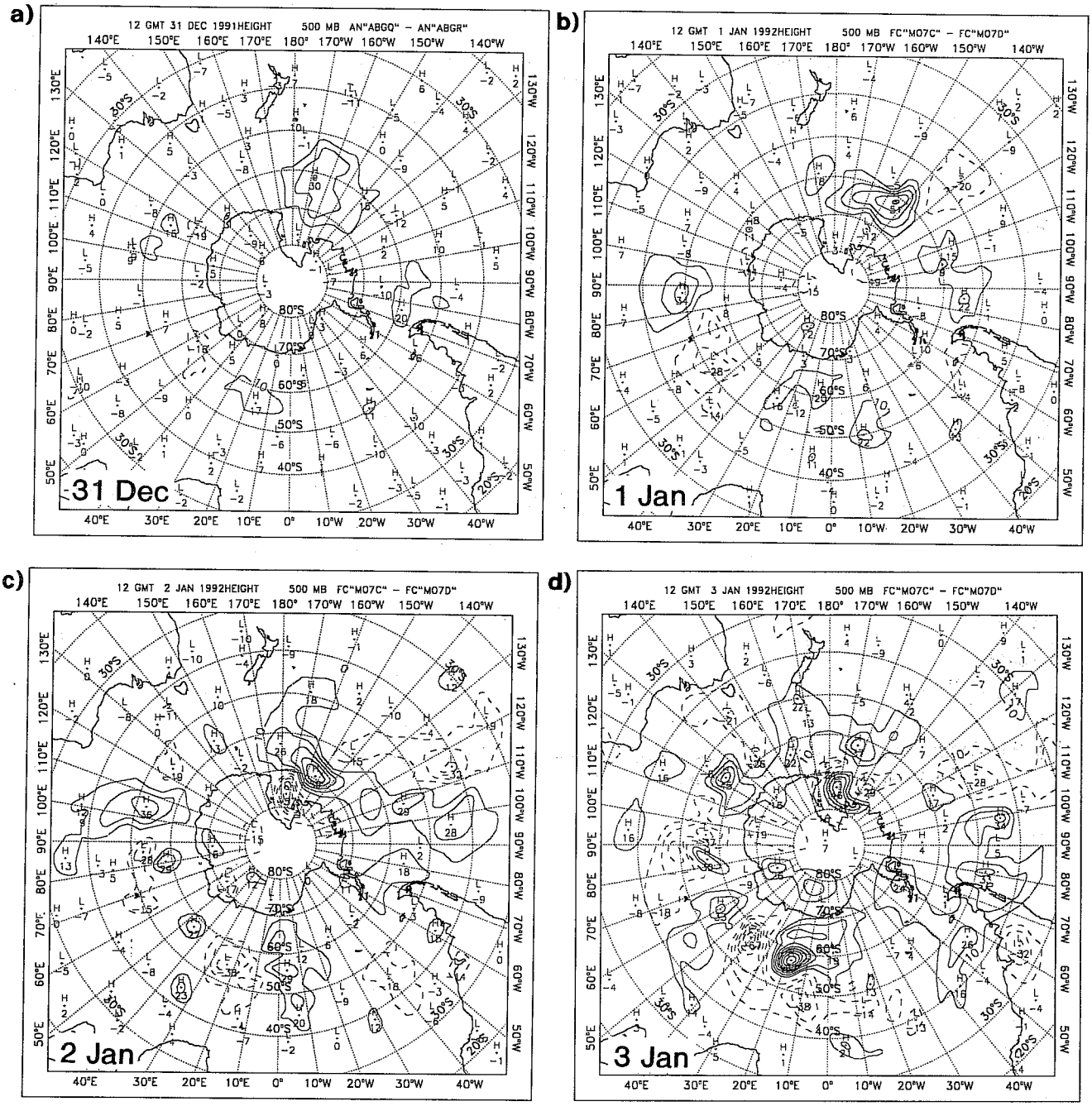

Fig. 25 SCATT - CONTROL analysis and forecast differences for the Southern Hemisphere 500 mb geopotential height for the forecast beginning 1200 GMT 31 December for (a) the analysis and for forecasts of (b) 24 h, (c) 48 h and (d) 72 h. (10 m contour interval.) Note that (d) is the difference of the bottom right 2 panels of Fig. 24.

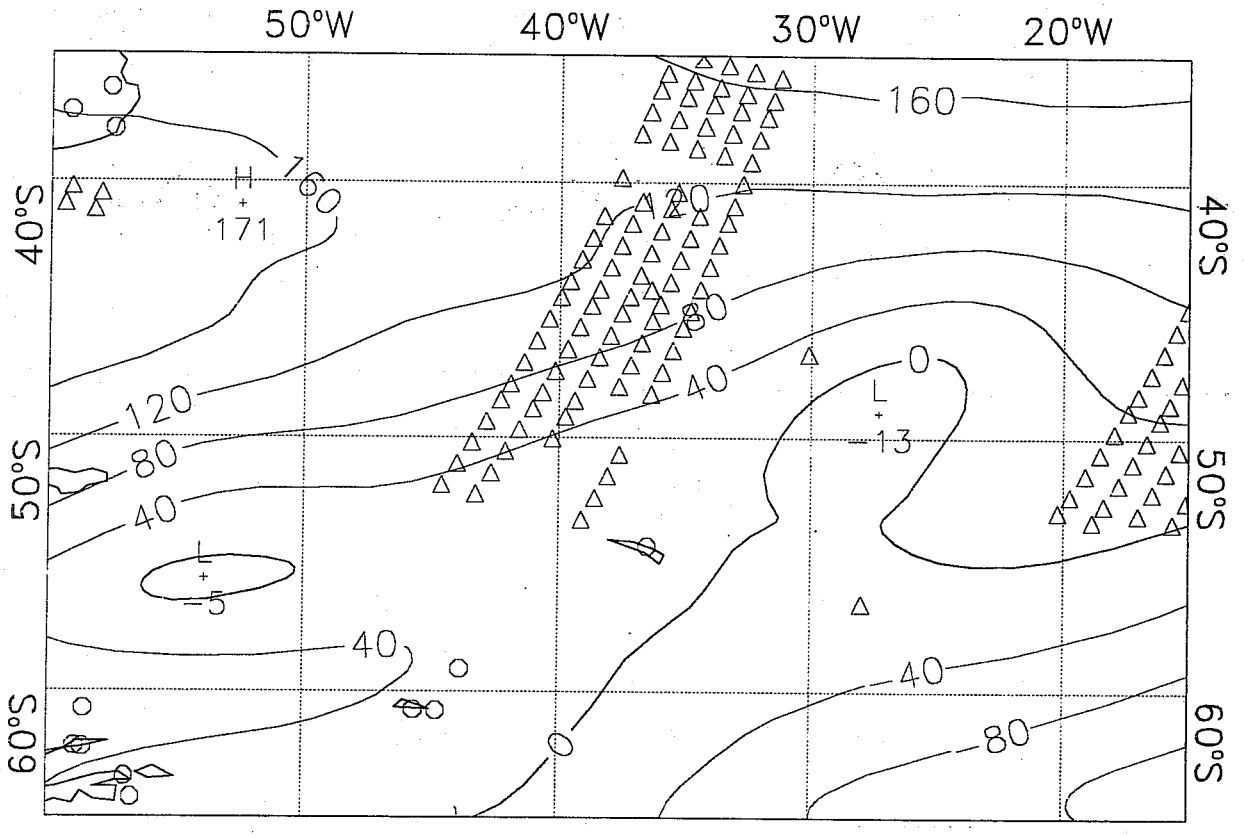

Fig. 26 Scatterometer data and the 1000 mb geopotential height SCATT analysis (40 m contour interval) for 1200 GMT 31 December for the South Atlantic.

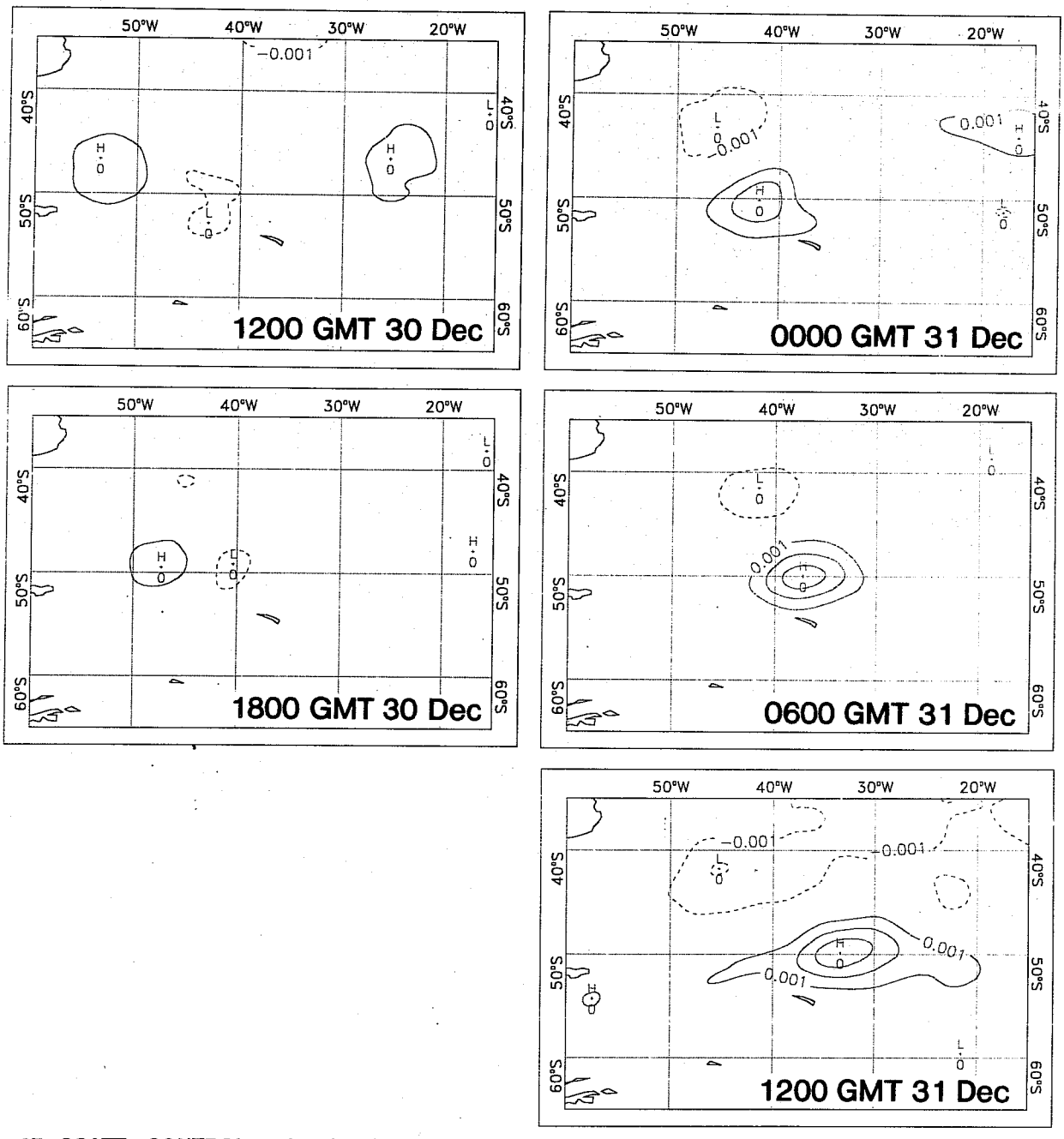

Fig. 27 SCATT - CONTROL analyzed surface pressure differences in the South Atlantic every 6 hours for 1200 GMT 30 to 31 December. (1 mb contour interval.)

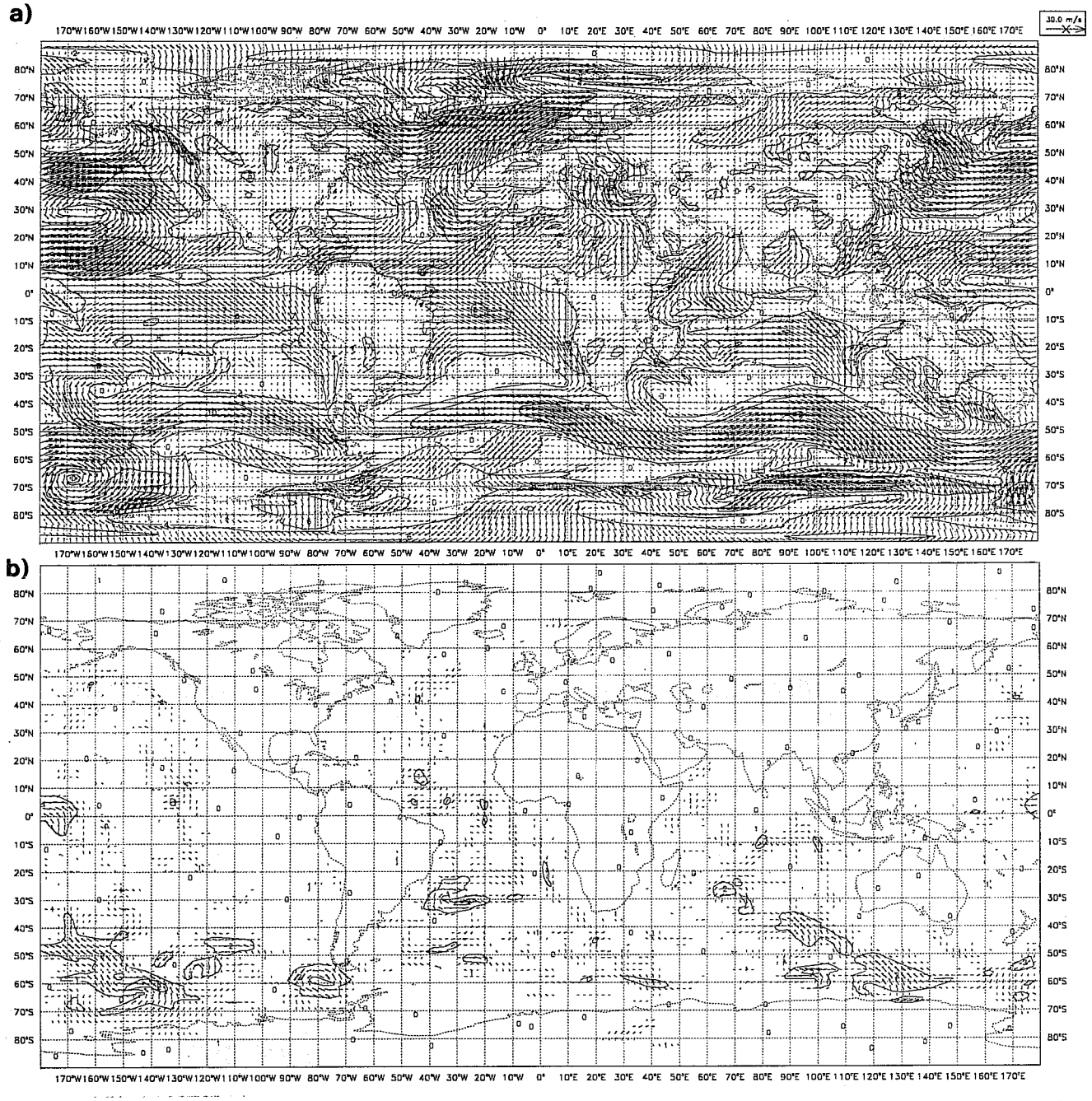

Fig. 28 Five day mean wind analyses for the lowest model level for (a) CONTROL and (b) SCATT - CONTROL. (4 and 1 m/s contour intervals.)

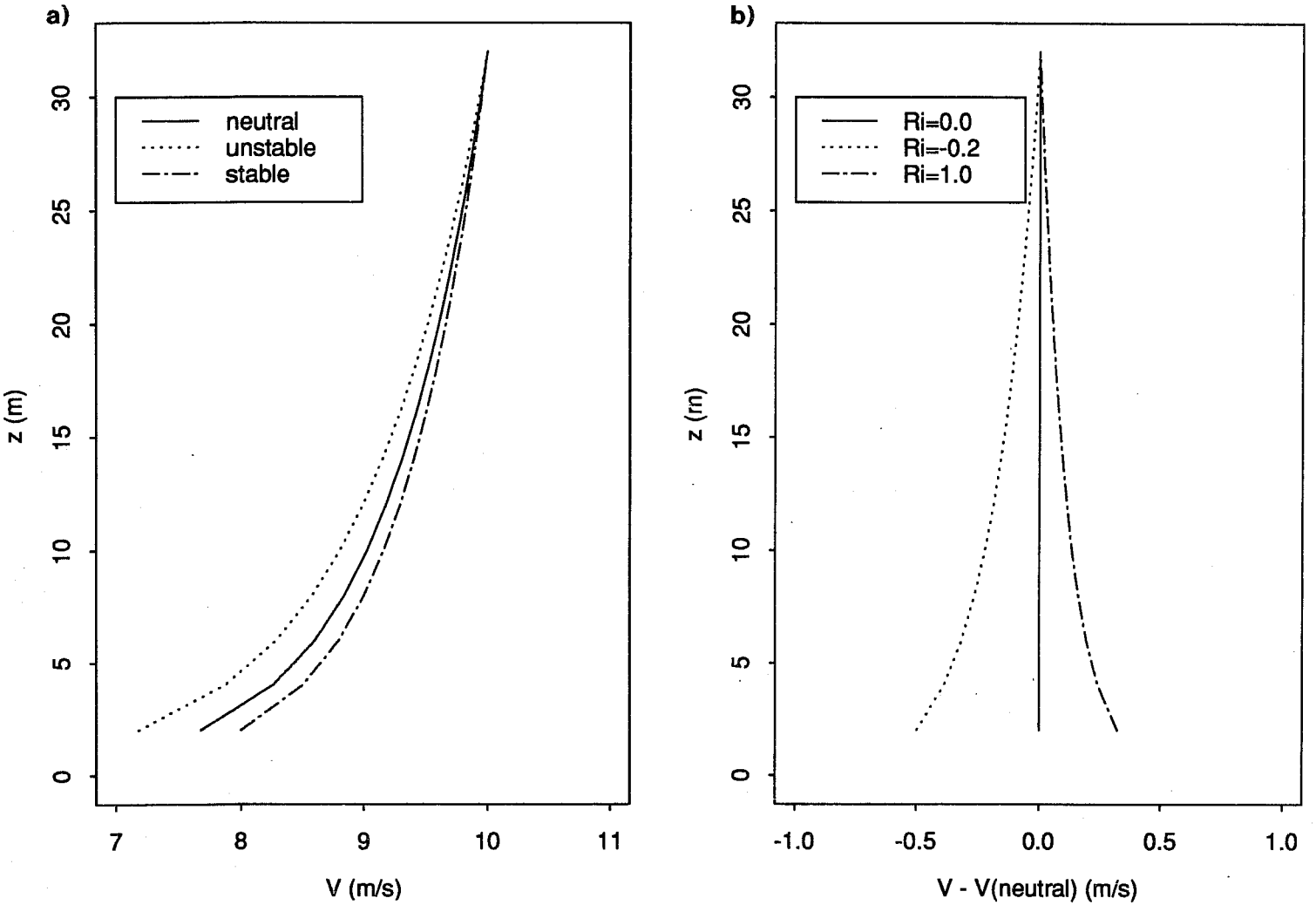

Fig. 29 The effect of stability on the vertical profile of wind in the boundary layer. The wind is taken to be 10 m/s at 32 m above the surface. The neutral, unstable and stable cases correspond to Richardson numbers of 0.0, -0.2 and 1.0. Both (a) the profiles and (b) the difference from the neutral case are shown.

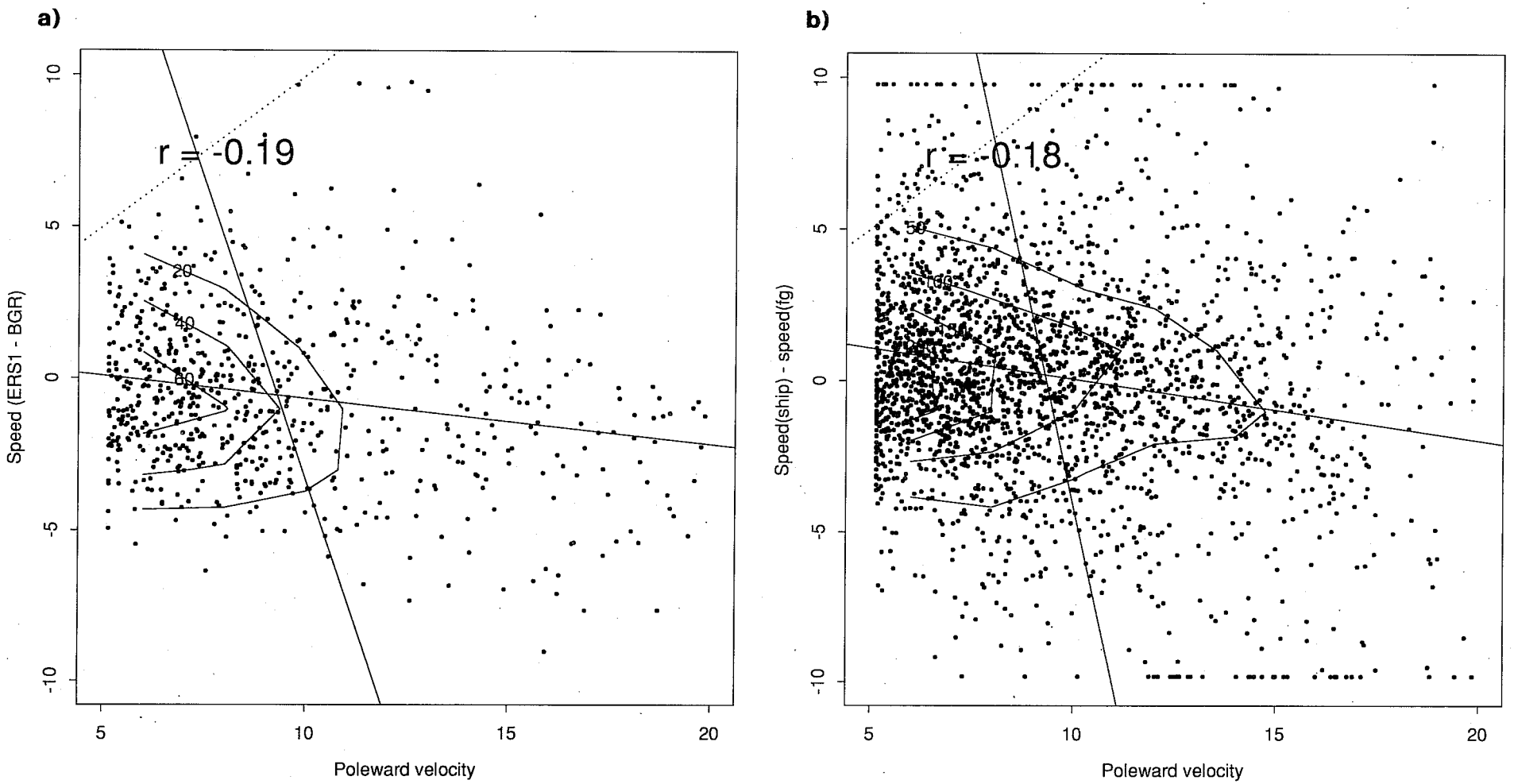

Fig. 30 Scatter plots of observed - model differences in speed versus model *v* wind component for (a) the scatterometer and (b) ships. Details are described in the text.

there is very little data and the analysis is very similar to the first guess. The evidence presented here is indirect, but is consistent with the conclusion that the scatterometer data improves the Southern Hemisphere surface wind analysis.

4. DISCUSSION AND CONCLUDING REMARKS

We have performed an observing system impact study of the ERS1 scatterometer data using the ECMWF data assimilation and forecast system. Notable features of our experimental configuration are:

- The model resolution is T106 in the horizontal and 19 layers in the vertical. The horizontal resolution of the analyses and forecasts is 200 km. (But see the discussion in Section 2.4 about horizontal resolution.)

- The CMOD2_Z model function is used. This is the CMOD2 formulation tuned to the ECMWF analyses by *Stoffelen and Anderson* (1992). This formulation was later modified to become the CMOD3 function implemented by ESA in the real-time retrievals from June 1992 onwards.

- CREO always uses the 6 hour forecast surface wind field as a reference field.

- Ice points (SST < 0°) are treated as land points by CREO.

- The scatterometer data are thinned to 100 km resolution before being passed to OI.

- A strict wind direction quality control is imposed - scatterometer winds differing by more than 60° relative to the 6 hour forecast winds are rejected.

- High accuracy is assumed for surviving scatterometer winds, equal to that of radiosondes (2.0 m/s for u and v wind components).

The impact of the scatterometer data is small. Analysis impacts do not build up during the experiment. At any one time, analysis impacts are substantial in the wind field up to 850 mb, trailing off to nearly nil by 500 mb. Mass field (i.e. geopotential height) impacts are small everywhere. Thus, the analysis tends to draw to the scatterometer data, without producing associated changes to the mass field. Differences between SCATT and CONTROL are little affected by the diabatic nonlinear normal mode initialization, but over the course of the 6 hour forecast within the data assimilation cycle, these differences are seen to decay very substantially. Our forecast impact results are not very surprising in light of this.

Forecast impacts are on balance neutral. Forecasts are quite similar out to 5 or 6 days, in the Northern Hemisphere. In the Southern Hemisphere, of the four cases, the scatterometer impact is positive once, neutral twice, and negative once. A larger experiment would be needed to conclude that the impact is either positive or negative overall. We are unable to directly link differences in a particular forecast feature with the absence or presence of scatterometer data. We have concluded that all the forecast impacts are basically

neutral. In any one case, considering any one feature, SCATT or CONTROL might be better or worse. Averaged over a hemisphere, the scores tend to even out. Averaged over a hemisphere and the four cases, the scores can hardly be distinguished.

Indirect evidence has been presented (Section 3.3) that the Southern Hemisphere low level wind analysis is improved under conditions of warm air advection. It appears that in the Southern Hemisphere, the scatterometer data corrects the tendency of the model to overestimate the wind speed in such cases.

Our study has some implications for future work.

- The data impacts are essentially neutral. The data processing and analysis procedures must be improved before operational use of the ERS1 scatterometer data begins.

- To improve the use of the scatterometer data within the OI context, the following need investigation (in order of decreasing importance):

  i) Tuning the OI to make more use of the scatterometer data in the analysis of the mass field. The ECMWF analysis relates wind and mass fields through the geostrophic relationship. The strength of this coupling is roughly 80% of full geostrophic coupling. Increasing this coupling may help, although boundary layer winds are generally in a state of geostrophic balance which is significantly modified by the friction force (*Schaefer and Doswell*, 1980)

  ii) Improve CREO. The quality control inherent in CREO is responsible for most of the scatterometer data rejections in these experiments. Recall, CREO generates two horizontally coherent wind fields from the ambiguous winds. In regions of relatively smooth flow, these two fields will be 180° out of phase and will be the only reasonable fields. In regions of more complicated flow several reasonable alternatives may be possible. Data is then tossed because neither of the two fields generated is similar to the first guess, either because the first guess is totally wrong or because neither of the fields generated is the 'right' one. A procedure based on median filtering (*Schultz*, 1990) initialized with the ambiguity closest to the first guess might prove more successful.

  iii) Improve the model function, accounting for stability effects and/or wave effects.

It is worth noting that outside the OI context there are other, perhaps better, ways of making use of scatterometer data. In parallel to the experiments reported here, we have been developing procedures to use the ERS1 σ^0 data in the ECMWF variational analysis system (based on *Talagrand and Courtier*, 1987,

Courtier and Talagrand, 1987, *Courtier and Talagrand*, 1990). Within this context the retrieval of ambiguous winds and the ambiguity removal are combined in one large data fitting problem which includes other observations, the first guess and balance constraints. This will be the ultimate version of the variational analysis method described some years ago by the author (*Hoffman*, 1982, 1984). In a static (3d) formulation, obtaining balancing mass field increments may still present a problem, but the variational formalism may allow more sophisticated balance constraints to be applied. In a dynamic (4D) formulation, differences between analyses will be differences between short term forecasts, and balancing mass field increments will be obtained necessarily (e.g. *Thépaut and Courtier*, 1991).

ACKNOWLEDGEMENTS

This work was supported by the NASA scatterometer project (Jet Propulsion Laboratory contract 957644, a subcontract to NASA contract NAS7-918) and by the ECMWF. (NASA is the United States National Aeronautics and Space Agency.) The facilities and hospitality of the ECMWF, in general and of the Research Department in particular, were indispensable for this work. I especially thank Per Undén who kindly answered my numerous requests for help during the course of the experiments described here.

References

Anderson, D., A. Hollingsworth, S. Uppala, and P. Woiceshyn. 1987: A study of the feasibility of using sea and wind information from the ERS-1 satellite, Part 1: Wind scatterometer data. Technical report, ECMWF, Reading, U.K. Contract 6297/86/HGE-I(SC), ESRIN.

Anderson, D., A. Hollingsworth, S. Uppala, and P. Woiceshyn, 1991a: A study of the use of scatterometer data in the European Centre for Medium-range Weather Forecasts operational analysis-forecast model. 1. Quality assurance and validation. J.Geophys.Res., 96(C2), 2619-2634.

Anderson, D., A. Hollingsworth, S. Uppala, and P. Woiceshyn., 1991b: A study of the use of scatterometer data in the European Centre for Medium-range Weather Forecasts operational analysis-forecast model. 2. Data impact. J.Geophys.Res., 96(C2), 2635-2647

Atlas, R., S. Peteherych, P. Woiceshyn, and M. Wurtele, 1982: Analysis of satellite scatterometer data and its impact on weather forecasting. Oceans, 415-420.

Baker, W.E., R. Atlas, E. Kalnay, M. Halem, P.M. Woiceshyn, S. Peteherych, and D. Edelmann, 1984: Large-scale analysis and forecast experiments with wind data from the Seasat-A scatterometer. J.Geophys.Res., 89(D3), 4927-4936.

Cane, M.A., V.J. Cardone, M. Halem, and I. Halberstam, 1981: On the sensitivity of numerical weather prediction to remotely sensed marine surface wind data: A simulation study. J.Geophys.Res., 86(C9), 8093-8106.

Cavanié, A. and P. Lecomte, 1987a: Vol 1. Study of a method to dealias winds from ERS-1 data. Final Report, European Space Agency. Contract 6874/87/CP-I(SC).

Cavanié, A. and P. Lecomte, 1987b: Vol 2. Wind retrieval and dealiasing subroutines. Final Report, European Space Agency. Contract 6874/87/CP-I(SC).

Courtier, P. and O. Talagrand, 1990: Variational assimilation of meteorological observations with the direct and adjoint shallow-water equations. Tellus, 42A, 531-549.

Courtier, P. and O. Talagrand. 1987: Variational assimilation of meteorological observations with the adjoint vorticity equation. Part 2: Numerical results. Q.J.Roy.Meteor.Soc., 113, 1329-1368.

Duffy, D., R. Atlas, T. Rosmond, E. Barker, and R. Rosenberg, 1984: The impact of Seasat scatterometer winds on the Navy's operational model. J.Geophys.Res., 89(D5), 7238-7244.

Duffy, D.G. and R. Atlas, 1986: The impact of Seasat-A scatterometer data on the numerical prediction of the Queen Elizabeth II storm. J.Geophys.Res., 91(C2), 2241-2248.

Francis, R., G. Graf, P. G. Edwards, M. McCaig, C. McCarthy, P. Dubock, A. Lefebvre, B. Pieper, P.-Y. Pouvreau, R. Wall, F. Wechsler, J. Louet, and R. Zobl, 1991: The ERS-1 spacecraft and its payload. ESA Bulletin, No.65, 27-48. ERS-1 Special Issue.

Graham, R., D. Anderson, A. Hollingsworth, and H. Böttger, 1989: Evaluation of ERS-1 wind extraction and ambiguity removal algorithms. Meteorological and statistical evaluation. ECMWF Reoprt to ESA, Reading, U.K.

Grantham, W.L., E.M. Bracalente, W.L. Jones, and J.W. Johnson, 1977: The Seasat-A satellite scatterometer. IEEE J.Ocean Engin., OE-2, 200--206.

Hoffman, R., 1982: SASS wind ambiguity removal by direct minimization. Mon.Wea.Rev., 110, 434--445.

Hoffman, R.N., 1984: SASS wind ambiguity removal by direct minimization. II: Use of smoothness and dynamical constraints. Mon.Wea.Rev., 112, 1829--1852.

Lenzen, A.J., D.R. Johnson, and R. Atlas, 1992: Analysis of the impact of Seasat scatterometer data and horizontal resolution on GLA model simulations of the QE II storm. Mon.Wea.Rev. *to be published*

Long, A.E., 1985: Towards a C-band radar sea echo model for the ERS-1 scatterometer. In: Conference on Spectral Signatures, Les Arcs, December 1985. ESA SP-247.

Long, A.E., 1991: Summary of Cmod2, Wismann, Cmod2_W & Cmod2_1 models. Document Number ESTEC/WMA/AEL/9101, Revision 1, ESTEC, European Space Agency, 28 February 1991.

Lönnberg, P., 1988: Developments in the ECMWF analysis system. In: Seminar on Data Assimilation Systems and the Use of Satellite Data, Reading, U.K., 1988. ECMWF, pp 75-120,

Lönnberg, P., J. Pailleux, and A. Hollingsworth, 1988: The new analysis system. Technical Memorandum 125, ECMWF, Reading, U.K.

Lönnberg, P., D. Shaw, and P Undén (editors), 1992: Research Manual 1, ECMWF Data Assimilation, Scientific Documentation. ECMWF, Reading, U.K.

Lorenc, A., 1981: A global three-dimensional multivariate statistical interpolation scheme. Mon.Wea.Rev., 109, 701-721.

Louis, J-F., 1979: A parametric model of vertical eddy fluxes in the atmosphere. Bound.-Layer Meteor., 17, 187-202.

Machenhauer, B., 1977: On the dynamics of gravity oscillations in a shallow water model with applications to normal mode initialization. Beitr. Phys. Atmosph., 50, 253-271.

Price, J.C., 1976: The nature of multiple solutions for surface wind speed over the oceans from scatterometer measurements. Remote Sens.Environ., 5, 47-54.

Schaefer, J.T., and C. A. Doswell, III, 1980: The theory and practical application of antitriptic balance. Mon.Wea.Rev., 108, 746-756.

Schultz, H., 1990: A circular median filter approach for resolving directional ambiguities in wind fields retrieved from spaceborne scatterometer data. J. Geophys.Res., 95(C4), 5291-5304.

Shaw, D.B., P. Lönnberg, A. Hollingsworth, and P. Undén, 1987: The 1984/85 revisions of the ECMWF assimilation system. Q.J.Roy.Meteor.Soc., 113, 533-566.

Simmons, A.J., D. M. Burridge, M. Jarraud, C. Girard, and W. Wergen, 1989: The ECMWF medium-range prediction models. Development of the numerical formulations and the impact of increased resolution. Meteor.Atmos.Phys., 40, 28-60.

Stoffelen, A., and D.L.T. Anderson, 1992: ERS-1 scatterometer calibration and validation activities at ECMWF: A. The quality and characteristics of the radar backscatter measurements. In: European 'International Space Year' Conference, Munich, Germany, 30 March - 5 April 1992.

Stoffelen, A., D.L.T. Anderson, and P. M. Woiceshyn, 1992: ERS-1 scatterometer calibration and validation activities at ECMWF: B. From radar backscatter characteristics to wind vector solutions. In: European 'International Space Year' Conference, Munich, Germany, 30 March - 5 April 1992.

Stoffelen, A.C.M., and G. J. Cats, 1991: The impact of Seasat-A scatterometer data on high-resolution analysis and forecasts: The development of the QE II storm. M.Wea.Rev., 119, 2794-2802.

Talagrand, O., and P. Courtier, 1987: Variational assimilation of meteorological observations with the adjoint vorticity equation. Part 1: Theory. Q.J.Roy.Meteor.Soc., 113, 1311-1328.

Thépaut, J.-N., and P. Courtier, 1991: Four-dimensional variational data assimilation using the adjoint of a multilevel primitive equation model. Technical Memorandum 178, ECMWF, Reading, U.K., February 1991. Submitted to Q.J.Roy.Meteor.Soc.

Undén, P., 1989: Tropical data assimilation and analysis of divergence. Mon.Wea.Rev., 117, 2495-2517.

Wergen, W., 1987: Diabatic nonlinear normal mode initialization for a spectral model with a hybrid vertical coordinate. Technical Report 59, ECMWF, Reading, U.K., 1987.

Yu, T.W., and R.D. McPherson, 1984: Global data assimilation experiments with scatterometer winds from SEASAT-A. Mon.Wea.Rev., 112, 368-376.

LIST OF ECMWF TECHNICAL REPORTS

1	A case study of a ten day forecast. (1976)	Arpe, K., L. Bengtsson, A. Hollingsworth, and Z. Janjic
2	The effect of arithmetic precision on some meteorological integrations. (1976)	Baede, A.P.M., D. Dent, and A. Hollingsworth
3	Mixed-radix Fourier transforms without reordering. (1977)	Temperton, C.
4	A model for medium range weather forecasts - adiabatic formulation. (1977)	Burridge, D.M., and J. Haseler
5	A study of some parameterisations of sub-grid processes in a baroclinic wave in a two dimensional model. (1977)	Hollingsworth, A.
6	The ECMWF analysis and data assimilation scheme: analysis of mass and wind field. (1977)	Lorenc, I. Rutherford and G. Larsen
7	A ten-day high-resolution non-adiabatic spectral integration; a comparative study. (1977)	Baede, A.P.M., and A.W. Hansen
8	On the asymptotic behaviour of simple stochastic-dynamic systems. (1977)	Wiin-Nielsen, A.
9	On balance requirements as initial conditions. (1978)	Wiin-Nielsen, A.
10	ECMWF model parameterisation of sub-grid scale processes. (1979)	Tiedtke, M., J.-F. Geleyn, A. Hollingsworth, and J.-F. Louis
11	Normal mode initialization for a multi-level grid-point model. (1979)	Temperton, C., and D.L. Williamson
12	Data assimilation experiments. (1978)	Seaman, R.
13	Comparison of medium range forecasts made with two parameterisation schemes. (1978)	Hollingsworth, A., K. Arpe, M. Tiedke, M. Capaldo, H. Savijarvi, O. Akesson, and J.A. Woods
14	On initial conditions for non-hydrostatic models. (1978)	Wiin-Nielsen, A.C.
15	Adiabatic formulation and organization of ECMWF's spectral model. (1979)	Baede, A.P.M., M. Jarraud, and U. Cubasch
16	Model studies of a developing boundary layer over the ocean. (1979)	Økland, H.
17	The response of a global barotropic model to forcing by large scale orography. (1980)	Quiby, J.
18	Confidence limits for verification and energetic studies. (1980)	Arpe, K.
19	A low order barotropic model on the sphere with orographic and newtonian forcing. (1980)	Kallen, E.
20	A review of the normal mode initialization method. (1980)	Du Xing-yuan
21	The adjoint equation technique applied to meteorological problems. (1980)	Kontarev, G.
22	The use of empirical methods for mesoscale pressure forecasts. (1980)	Bergthorsson, P.
23	Comparison of medium range weather forecasts made with models using spectral or finite difference techniques in the horizontal. (1981)	Jarraud, M., C. Girard, and U. Cubasch
24	On the average errors of an ensemble of forecasts. (1981)	Derome, J.

25	On the atmospheric factors affecting the Levantine Sea. (1981)	Ozsoy, E.
26	Tropical influences on stationary wave motion in middle and high latitudes. (1981)	Simmons, A.J.
27	The energy budgets in North America, North Atlantic and Europe based on ECMWF analysis and forecasts. (1981)	Sävijärvi, H.
28	An energy and angular momentum conserving finite-difference scheme, hybrid coordinates and medium range weather forecasts. (1981)	Simmons, A.J., and R. Strufing
29	Orographic influences on Mediterranean lee cyclogenesis and European blocking in a global numerical model. (1982)	Tibaldi, S. and A. Buzzi
30	Review and re-assessment of ECNET - A private network with open architecture. (1982)	Haag, A., Königshofer, F. and P. Quoilin
31	An investigation of the impact at middle and high latitudes of tropical forecast errors. (1982)	Haseler, J.
32	Short and medium range forecast differences between a spectral and grid point model. An extensive quasi-operational comparison. (1982)	Girard, C. and M. Jarraud
33	Numerical simulations of a case of blocking: The effects of orography and land-sea contrast. (1982)	Ji, L.R., and S. Tibaldi
34	The impact of cloud track wind data on global analyses and medium range forecasts. (1982)	Källberg, P., S. Uppala, N. Gustafsson, and J. Pailleux
35	Energy budget calculations at ECMWF. Part 1: Analyses 1980-81. (1982)	Oriol, E.
36	Operational verification of ECMWF forecast fields and results for 1980-1981. (1983)	Nieminen, R.
37	High resolution experiments with the ECMWF model: a case study. (1983)	Dell'Osso, L.
38	The response of the ECMWF global model to the El-Niño anomaly in extended range prediction experiments. (1983)	Cubasch, U.
39	On the parameterisation of vertical diffusion in large-scale atmospheric models. (1983)	Manton, M.J.
40	Spectral characteristics of the ECMWF objective analysis system. (1983)	Daley, R.
41	Systematic errors in the baroclinic waves of the ECMWF. (1984)	Klinker, E., and M. Capaldo
42	On long stationary and transient atmospheric waves. (1984)	Wiin-Nielsen, A.C.
43	A new convective adjustment. (1984)	Betts, A.K., and M.J. Miller
44	Numerical experiments on the simulation of the 1979 Asian summer monsoon. (1984)	Mohanty, U.C., R.P. Pearce and M. Tiedtke
45	The effect of mechanical forcing on the formation of a mesoscale vortex. (1984)	Guo-xiong Wu and Shou-jun Chen
46	Cloud prediction in the ECMWF model. (1985)	Slingo, J., and B. Ritter
47	Impact of aircraft wind data on ECMWF analyses and forecasts during the FGGE period, 8-19 November. (1985)	Baede, A.P.M., P. Källberg, and S. Uppala

48	A numerical case study of East Asian coastal cyclogenesis. (1985)	Chen, Shou-jun and L. Dell'Osso
49	A study of the predictability of the ECMWF operational forecast model in the tropics. (1985)	Kanamitsu, M.
50	On the development of orographic. (1985)	Radinovic, D.
51	Climatology and systematic error of rainfall forecasts at ECMWF. (1985)	Molteni, F., and S. Tibaldi
52	Impact of mofified physical processes on the tropical simulation in the ECMWF model. (1985)	Mohanty, U.C., J.M. Slingo and M. Tiedtke
53	The performance and systematic errors of the ECMWF tropical forecasts (1982-1984). (1985)	Heckley, W.A.
54	Finite element schemes for the vertical discretization of the ECMWF forecast model using linear elements. (1986)	Burridge, D.M., J. Steppeler, and R. Strüfing
55	Finite element schemes for the vertical discretization of the ECMWF forecast model using quadratic and cubic elements. (1986)	Steppeler, J.
56	Sensitivity of medium-range weather forecasts to the use of an envelope orography. (1986)	Jarraud, M., A.J. Simmons and M. Kanamitsu
57	Zonal diagnostics of the ECMWF operational analyses and forecasts. (1986)	Branković, Č.
58	An evaluation of the performance of the ECMWF operational forecasting system in analysing and forecasting tropical easterly disturbances. Part 1: Synoptic investigation. (1986)	Reed, R.J., A. Hollingsworth, W.A. Heckley and F. Delsol
59	Diabatic nonlinear normal mode initialisation for a spectral model with a hybrid vertical coordinate. (1987)	Wergen, W.
60	An evaluation of the performance of the ECMWF operational forecasting system in analysing and forecasting tropical easterly wave disturbances. Part 2: Spectral investigation. (1987)	Reed, R.J., E. Klinker and A. Hollingsworth
61	Empirical orthogonal function analysis in the zonal and eddy components of 500 mb height fields in the Northern extratropics. (1987)	Molteni, F.
62	Atmospheric effective angular momentum functions for 1986-1987. (1989)	Sakellarides, G.
63	A verification study of the global WAM model December 1987 - November 1988. (1989)	Zambresky, L.
64	Impact of a change of radiation transfer scheme in the ECMWF model. (1989)	Morcrette, J-J.
65	The ECMWF analysis-forecast system during AMEX. (1990)	Puri, K., P. Lönnberg and M. Miller
66	The calculation of geopotential and the pressure gradient in the ECMWF atmospheric model: Influence on the simulation of the polar atmosphere and on temperature analyses. (1990)	Simmons, A.J. and Chen Jiabin
67	Assimilation of altimeter data in a global third generation wave model (1992)	Lionello, P., H. Günther and P. Janssen
68	Implementation of a third generation ocean wave model at the European Centre for Medium-Range Weather Forecasts (1992)	Günther, H., P. Lionello, P.A.E.M. Janssen et al.